AD 688940

BIOLOGICAL AND RADIOLOGICAL EFFECTS OF

FALLOUT FROM NUCLEAR EXPLOSIONS

Chapter 3

Distribution of Local Fallout

MAY 1969

OCD Work Unit 3119B

JUN 1 3 1969

URS SYSTEMS CORPORATION

10'

BIOLOGICAL AND RADIOLOGICAL EFFECTS OF FALLOUT FROM NUCLEAR EXPLOSIONS

Chapter 3

Distribution of Local Fallout

MAY 1969

OCD Work Unit 3119B

by

Carl F. Miller

URS RESEARCH COMPANY
1811 Trousdale Drive
Burlingame, California 94010

for

OFFICE OF CIVIL DEFENSE
Office of the Secretary of the Army
Washington, D.C. 30210

through

Technical Planning and Management Office
Naval Radiological Defense Laboratory
San Francisco, California 94135

URS 702-1
TRC 68-61

BIOLOGICAL AND RADIOLOGICAL EFFECTS OF FALLOUT FROM NUCLEAR EXPLOSIONS
Chapter 3, Distribution of Local Fallout
by Carl F. Miller, May 1969

Prepared by URS Research Company
1811 Trousdale Drive, Burlingame, California 94010

Under Contract No. N00228-68-C-2390
OCD Work Unit 3119B

SUMMARY REPORT

This report summarizes the fallout pattern scaling relationships that were developed in the period 1962 to 1964; the report includes the values of the scaling equation coefficients that were derived from selected fallout pattern data. The meaning of the scalar wind speed multiplier that is used in the scaling equations is discussed relative to computer applications of the scaling system and approximate wind speed adjustment factors for use with wind speed averages that may be assumed in such applications are provided. The relative degree of wind shear inherent in the scaling system parameters is also discussed in some detail. Basic equations for relating surface density of radionuclides and air ionization rates, including consideration of fractionation, surface roughness, and instrument response, are given and discussed together with the influence of these factors and others on the limiting values of K factors that represent the relative amount of the radioactive sources contained within the deduced area covered by the fallout patterns. Scaling equations and data are also presented for use in estimating, for any location in the fallout region, the time of fallout arrival, the time of fallout cessation, the variation of the exposure rate (i.e., air ionization rate in roentgens per hour) with time during fallout arrival, and the total exposure from the time of fallout arrival to selected later times.

FOREWORD

The major content of this report was developed by the author in the period 1962 to 1964 and, in draft form, the material has been available to computer programmers at the Stanford Research Institute (Menlo Park, California) and at the American Research Corporation (Fullerton, California). The computer programs, in turn, have been available to the Office of Civil Defense, their contractors, and others. In some cases programming simplifications and interpolation schemes have been added to decrease computing time or for other reasons. Since such changes can become iterative with respect to departures from the original systems, and since without the original scaling functions, the program user has no means of checking the program output, it was requested that the original scaling equations be reported for record and for computer program verification.

In preparing the report for publication, a few changes in scaling functions were made, mainly on the procedures for estimating the time of arrival and rate of arrival of the fallout from cloud heights. Also, a few out-of-date assumptions, statements, and conclusions were deleted or revised. New work reported elsewhere (such as that sponsored by the Defense Atomic Support Agency, Department of Defense) since 1964 is not discussed nor is reference made to such studies, since the results therefrom were not available for the analytical results summarized in this report.

Some question still exists with respect to the appropriate value of a wind speed that should be applied in the calculations to conform with the total and angular shear effects included in the derived scaling functions. To clarify this question, particle displacement calculations have been added, discussed, and a first order wind speed adjustment factor is suggested for use when an average wind speed is assumed; the details of the discussion on this question are given in paragraph 3.5.4.

CONTENTS

ILLUSTRATIONS

TABLES

Chapter 3
DISTRIBUTION OF LOCAL FALLOUT

3.1 Background

3.1.1 The Distribution Process

A very simple descriptive statement of the fallout process is that a cloud of particles is formed rapidly as the result of an explosion and that this cloud is then dispersed by the wind and by the force of gravity acting on the particles to return them to the earth. Most treatments of distribution of fallout assume that the visible volume occupied by the nuclear cloud and stem above the point of detonation within a few minutes after explosion more or less defines the volume source of the fallout particles.[1] One treatment,[2] however, considers the particle source volume contained within the air volume swept through by the rising fireball. In either case the source volumes for the particles depend on total yield and, if other than surface detonations are considered, on the height or depth of burst. The yield-dependent parameters which are used to define the particle source geometry include the cloud height, cloud thickness and radius, and, occasionally, the stem geometry, and the time dependence of these parameters.

One important additional factor that is usually considered in the fallout distribution process is the spatial concentration of the particles in the volume; also qualitative considerations have been given to internal circulations of the particles by several investigators.[3,4] The discussion in Reference 4 on this circulation is summarized in this chapter.

The fall trajectory of a particle through the atmosphere depends on its own properties and on meteorological factors. The various aspects of these factors have been discussed by Schuert,[5] Anderson,[2] and others.[1] The major properties that influence a particle's fall rate through the atmosphere are its density, diameter or size, and shape. The major meteorological factors are the wind speed and direction and the air density and viscosity as a function of altitude.

1

The two air properties, of course, are dependent on the air pressure and temperature, and these, in turn, change with altitude. The wind speed and direction are also highly variable quantities, since each has both spatial and time variations. The vertical motions of the air and particle-group diffusion can influence the fall trajectory of particles but are usually not taken into account in the study of the fallout distribution process.

It is often found that when the observed cloud rates of rise (or the stabilized cloud heights) and the particle fall rates are used to compute the time of arrival of particles at locations very close to ground zero where fallout from stem altitudes should predominate, the calculated arrival times are quite consistently longer than the observed arrival times. Actually, the same discrepancy is often observed for cloud fallout at larger distances.

The consistency of the longer computed arrival time for particles falling near ground zero suggests that when the rising cloud takes on a toroidal motion, the larger particles are thrown from the gas mass and experience downward accelerations for some rather extended period of time. Because the calculated fall rates include only accelerations due to gravity, the computed time of fall (neglecting downward accelerations) from the height of the cloud would always be longer than the true time. Conversely, when the fall rates are used in order to estimate the height of origin of a particle from the time of its arrival on the ground (including its rise time), the computed height of origin i less than the cloud height.

This interpretation of the above-mentioned observations of particle arrival time may be used to describe, in qualitative terms, the process of stem fallout. The rising fireball takes on toroidal circulation as it rises from the surface of the ground, and this circulation persists through transition to cloud form until the internal pressures and temperatures of the system approach those of the ambient air, thereby establishing a large-scale air circulation. Air and soil particles rise from directly below the cloud in a narrow visible stem or chimney, and the surrounding air is entrained over the whole length of this stem. This rising material flows into the

2

bottom center of the cloud, and the countercurrent air flow, around the
periphery of the cloud, is downward. The observable effect, upon occasion,
is that the mass of particles appears to flow out from the top portion of
the cloud and then downward. As the cloud approaches its maximum height,
the circulation pattern apparently rapidly disintegrates or breaks up into
segregated regions of turbulence under influence of the ambient meteorological
forces.

When the toroidal circulation starts, a particle (or liquid drop) in the
central region of the cloud would, by centrifugal force, be moved to the outer
periphery of the cloud and then be accelerated downward at speeds greater than
the particle's normal fall velocity; it would then be at a lower altitude than
the cloud when its terminal fall velocity is reached. Even if this centrif-
ugal action and movement to the exterior of the rising cloud did not occur for
the majority of the particles, they could still fall from lower altitudes, by
virtue of the downward circulation around the periphery of the cloud, than
would be calculated on the basis that gravity-pull alone was overcoming the
gross rise rate of the visible cloud.

However, even with toroidal motion, the separation of fallout particles
by size because of gravity forces is still a valid concept. The smaller
particles will not move outward by centrifugal forces as far as the larger
ones in the circulation, and they could be swept back upward through the
cloud as long as the velocity of the rising air is sufficiently large. This
type of particle source circulation and ejection can be used to explain the
observed change in radiochemical composition of different size particles
discussed in Chapter 2, Reference 6.

The major radiological factors in the fallout distribution process are
the fission yield and the variation with particle size of the gross radioac-
tivity carried by particles of a given size. The first essentially determines
the total radioactivity available for distribution on the particles; the second
involves the distribution of that radioactivity among particles of different
sizes.

3

3.1.2 Mathematical Representations

The original attempt to describe and/or predict the end result of the fallout distribution process — the fallout pattern — was made by C. F. Ksanda and coworkers in 1953.[7] The original scaling method was based on the work of Laurino and Poppoff,[8] which described some fallout patterns for low-yield devices derived from observed data obtained during Operation Jangle in 1951. The original scaling method was intended for predictions or estimates of fallout patterns from yields possibly as high as 10 KT. In 1955[9] the method was expanded to include yields in the megaton range, without adequate explicit experimental documentation. This method was subsequently included in ENW[10]; however, in the latest edition of this document, the fallout pattern scaling is revised. In many damage assessment studies of fallout effects, a scaling system is to be preferred over a complex mathematical model.

Mathematical models attempt to establish quantitative values for the several fallout distribution parameters mentioned above and to compute the activity deposited on the ground at various locations, usually through the use of electronic computers. The general approach used and the organizations and investigators involved in the development and testing of these models up to 1957 is described in some detail by Kellogg.[1] Later developments include the work by Anderson,[2,11] by Pugh and Galiano,[12] by Callahan et al.,[13] and by Rapp,[14] to mention a few of the unclassified reported studies. A general comment on the results might be that none of the models agree with each other in several details and that none of the models reproduce very accurately all of the few data in the yield range of 1 KT to 15 MT that are experimentally available.

The exact causes of the differences among the various models are difficult to isolate for at least two reasons:

1. Each model is different from any other in several of its assumptions about parameter values or in its manner of handling the many variables mathematically.

4

2. Generally, the reports describing the models do not
   include sufficient detailed information regarding the
   minor assumptions and the methods used in making the
   computations.

If the input data in the mathematical models were all more reliably estab-
lished experimentally, many of the differences among them would disappear.
Whether this would produce better agreement with observations would still
have to be established.

In mos mathematical models, after selection of the values of the source
geometry, trajectory, and radiological factors, the computation is carried
out by dividing the source geometry for each of several particle size ranges
into horizontal discs of finite thickness. The location on the ground where
these "particle discs" land, under the influence of stated meteorological
conditions, is then calculated. All the activity at each of a series of
coordinate points is then summed according to the number of different discs
that land at the point and the amount of activity assigned to each disc.

So short a summary of the work on the mathematical models should not be
interpreted to mean that the efforts in the development of the mathematical
models have been small and unfruitful. On the contrary, much has been
learned about the fallout process through them, and most of the concepts
employed by many of the mathematical model developments are covered in the
remainder of this chapter. But to describe all the work and all the details
of each model currently in use is not considered to be within the scope of
this discussion.

3.1.3 Fallout Pattern Features

Although observed data on fallout patterns from land-surface shots
of various yields are very meager, the processed data give indication in a
qualitatitive way of a number of persistent characteristics. For example, the
general shape of the fallout standard intensity contours (in R/hr at 1 hr)
from shots in which the wind structures were rather simple, resembles a shadow
of the mushroom cloud and its stem on the ground.

Because of the shortage of reliable data on the fallout patterns from land-surface detonations, any systematic method for scaling fallout patterns (i.e., methods for interpolating and/or extrapolating data from one weapon yield to another) must take full advantage of all such apparently persistent qualitative characteristics of the available patterns. In devising methods that can convert the qualitative characteristics to quantitative ones, the methods must, of course, be capable of at least reproducing the observed data used in obtaining the original scaling relationships, which are given as functions of weapon yield.

Some of the apparently persistent characteristics of the fallout patterns from surface detonations are:

1. In the region near ground zero, the intensity gradient in the upwind and crosswind directions is very steep.

2. The high intensities near ground zero appear as an intensity ridge (rather than as a circular peak) displaced in the downwind direction.

3. The length of this high intensity ridge appears to be proportional to the width of the lower portion of the stem.

4. The peak intensity of the ridge increases with yield in the 1- to 10-KT yield range and decreases in the 100-KT to 10-MT yield range.

5. The best simple empirical relationship for the variation of the intensity with upwind and crosswind distance from ground zero, from graphical plots of the data, is that the form $I_o e^{-kx}$, where I_o is the ridge peak intensity, k is a constant for a given yield, and x is the upwind and/or crosswind distance from the upwind shoulder of the ridge peak.

6. The contours downwind from ground zero appear to be parallel to the intensity ridge for its entire length.

7. At distances greater than the length of the ridge, the intensity contours directly downwind decrease with distance from ground zero.

8. At some distance downwind (or perhaps even upwind for very large yields), the low-valued intensity contours fan out, and the intensities directly downwind from ground zero rise sharply with distance and then more slowly with distance to a peak value.

6

9. The distance from ground zero to this downwind peak intensity increases with weapon yield.

10. The magnitude of the peak intensity also appears to increase continuously with yield.

11. The distance between the lower valued contours appears to be related to the width of the cloud (not considering wind shear differences), and the maximum width seems to occur farther downwind than the peak intensity.

12. The variation of the intensity with downwind distance from this outer pattern peak can be approximated within reasonable limits of error, if the form of the wind shear pattern is not complex, by a function of the form $I_o e^{-mx}$, where I_o is the peak intensity, m is a yield-dependent parameter, and x is the downwind distance from the peak.

The above-listed fallout pattern characteristics are based on a combination of experimental observations and analyses of field test data. The most reliable persistencies appear to be those numbered 1, 2, 4, 6, 7, 8, and 9.

3.1.4 Simplified Fallout Scaling System for Land-Surface Detonations

The fallout scaling system described here was developed for estimating standard intensities, potential exposure doses, and other radiological quantities by use of both manual and machine computational techniques. The system is based on corrected experimental data, on empirical relationships among the geometrical arrangement of the cloud and stem as the source of fallout particles, and on several of the observed features of the fallout pattern of radiation intensities on the ground. In the system, the cloud and stem dimensions are stylized as simple solid geometric configurations to facilitate the use of algebraic relationships among the model parameters and the dependence of the parameter values on weapon yield.

In making estimates of the hazards from fallout, for the purpose of establishing the nature and required degree of protection against these hazards, two major quantities requiring evaluation are (1) the exposure dose levels that can result at different distances from the detonation and (2) the land

7

surface area in which the exposure dose is greater than a stated amount. To
make these evaluations requires estimates of the amount of fallout that
deposits at various locations, the time at which the fallout arrives, and
the rate of its arrival.

Such general evaluations of radiological hazard levels and of the pro-
tection requirements for radiological countermeasures in defense planning
must first consider the possible levels of effect (or hazard) and, in a
generalized manner, the feasibility of methods for protecting against these
levels of possible hazard. For these purposes, a rather simplified fallout
scaling system can serve; no precise or accurate prediction of fallout under
specified detonation and wind conditions is needed or is possible, even with
the most complicated fallout models at their present stage of development.
Therefore in the following discussion the presentation is limited to the
description of a simplified version of the fallout distribution process.

The mathematical derivations of the simplified fallout scaling system
are designed to describe the fall of particles of different size-groups
from a volume source in the air; the boundaries of that source are assumed
to depend only on weapon yield. The problem is to describe mathematically
the dependence of the fallout pattern features, in space and time, on (a)
the cloud and stem geometry, (b) the particle fall velocities, (c) the wind
velocity, (d) the radioactivity-particle size distributions, and (e) the
weapon yield.

The geometrical configuration of the cloud for the scaling system is
an oblate spheroid, and the configuration of the stem is a frustum of an
exponential cone or horn whose larger base is approximately adjacent to the
bottom of the spheroid. The fall of particles from each of these source
volumes is considered separately. The mathematical description and detailed
assumptions used in the development of the model are given in Reference 4;
only those details needed for use of the derived pattern scaling functions
are presented in the following discussion.

8

Some of the pattern features of interest along the downwind axis (Y = 0) of the idealized fallout pattern are shown in Figure 3.1 as a schematic intensity profile. The numbers shown in the figure correspond to the numerical subscripts of the scaling functions. The evaluated scaling functions for these and other quantities are given in the following paragraphs as summarized from the data given in Reference 4. In the scaling system, the fallout patterns for the particles falling from stem altitudes and from cloud altitudes are computed separately; at locations where these two patterns overlap, the computed standard intensities are then added together. This is illustrated in Figure 3.1 by the dotted line between X_3 and X_6. The standard or reference condition for all the fallout pattern scaling functions presented in the following paragraphs and sections is 100 percent fission yield; the radioactive components assumed to be present are discussed in Paragraph 3.4.3.

3.2 Fallout Deposition from Stem Altitudes

3.2.1 Ground Zero Intensity Ridge

The ground zero intensity ridge is depicted in Figure 3.1 by the downwind distances X_2 and X_3 and the intensity $I_{2,3}$. The dependence of X_2 and X_3 on the average wind speed and weapon yield is represented by[*]

$$X_2 \simeq 0.0327W^{0.230}\left[v_w - 3.96W^{0.128}\right]\text{miles}; \quad W = 30 \text{ to } 10^5 \text{ KT} \qquad (3.1)$$

and

$$X_3 \simeq 0.0327W^{0.230}\left[v_w + 3.96W^{0.128}\right]\text{miles}; \quad W = 30 \text{ to } 10^5 \text{ KT} \qquad (3.2)$$

for v_w in miles per hour and W in kilotons total yield. The values of $I_{2,3}$ are estimated from

---

[*] Approximate equalities indicate smoothed logarithmic scaling functions; equal signs are used for the basic scaling functions assumed in the derivations.

X (RELATIVE UNITS)

STANDARD INTENSITY (RELATIVE UNITS)
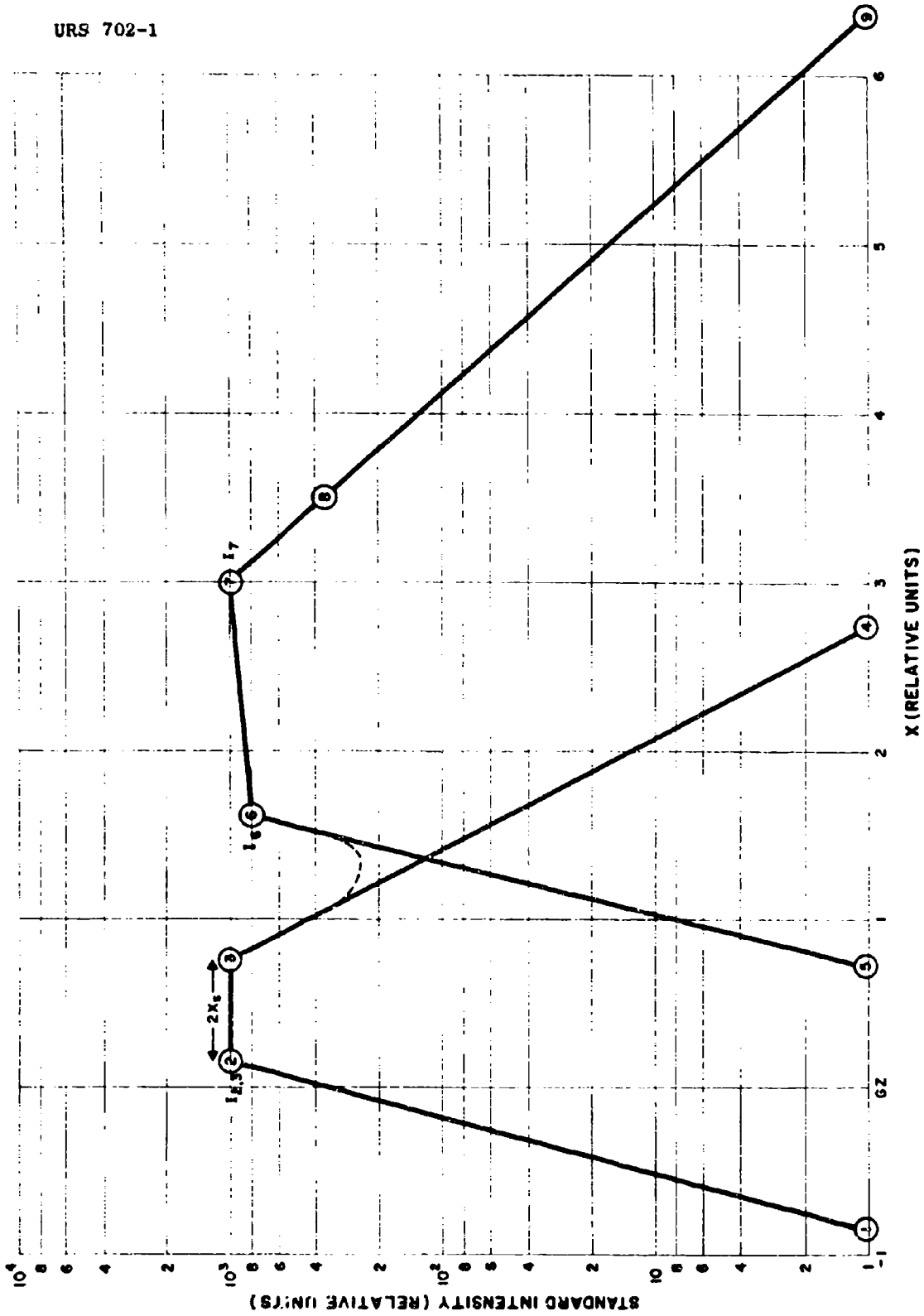
Fig. 3.1.   Schematic Outline for the Intensity Profile Downwind from Ground Zero Along the Axis of the Fallout Pattern (Y = 0) as used in the Simplified Fallout Pattern Scaling System

$$I_{2,3} = 3.02 \times 10^6 v_w^{-n_w} W^{-0.519} \text{ R/hr at 1 hr; } W = 30 \text{ to } 10^5 \text{ KT} \qquad (3.3)$$

where $I_{2,3}$ is the standard intensity for a 100 percent fission yield weapon, and n_w is an empirically derived yield-dependent parameter whose value is calculated from

$$n_w = 0.821 - 0.0191 \log W; \text{ } W = 30 \text{ to } 9,000 \text{ KT} \qquad (3.4)$$

or

$$n_w = 1.200 - 0.115 \log W; \text{ } W = 9 \times 10^3 \text{ to } 10^5 \text{ KT} \qquad (3.5)$$

The effective fall velocity vector for the median-diameter particles landing at $(X_2 + X_3)/2$ is given by

$$v_{f_{2,3}} = 68.3 W^{-0.080} \text{ ft/sec; } W = 1 \text{ to } 10^5 \text{ KT} \qquad (3.6)$$

The apparent height of origin of the particles with the fall velocity vector given by Equation 3.6 can be estimated from

$$z_{2,3} = 8.04 \times 10^3 W^{0.150} \text{ feet; } W = 30 \text{ to } 10^5 \text{ KT} \qquad (3.7)$$

3.2.2 Downwind Intensity Contours

The downwind distance to the location X_4 of Figure 3.1 on the center line of the stem pattern is given by

$$X_4 = 0.316 v_w W^{0.203} \text{ miles; } W = 30 \text{ to } 10^5 \text{ KT} \qquad (3.8)$$

The standard intensity, for a 100 percent fission yield weapon, associated with the downwind distance designated by X_4 is given by

$$I_4 = 15.0/v_w \qquad (3.9)$$

11

The downwind distances, X_c, to other intensity values, I_s, between $I_{2,3}$ and I_4 on the pattern centerline from X_3 to X_4 are estimated from

$$X_c = X_3 + \frac{(X_4 - X_3) \log (I_{2,3}/I_s)}{\log (I_{2,3}/I_4)} \qquad (3.10)$$

The effective fall velocity vector of the media-diameter particles landing at X_4 is given by

$$v_{f_4} = 13.8W^{-0.082} \text{ ft/sec}; \quad W = 1 \text{ to } 10^5 \text{ KT} \qquad (3.11)$$

The apparent height of origin of the particles with the fall velocity vector given by Equation 3.11 can be estimated from

$$z_4 \approx 1.57 \times 10^4 W^{0.121} \text{ feet}; \quad W = 30 \text{ to } 4 \times 10^4 \text{ KT} \qquad (3.12)$$

or

$$z_4 \approx 1.62 \times 10^4 W^{0.118} \text{ feet}; \quad W = 4 \times 10^4 \text{ to } 10^5 \text{ KT} \qquad (3.13)$$

3.2.3 Upwind Distance to the 1 R/hr at 1 hr Contour

The upwind distance to the 1 R/hr at 1 hr contour (i.e., I_1), designed by the numeral one in Figure 3.1 is estimated from

$$X_1 = -0.695W^{0.319} \text{ miles}; \quad W = 30 \text{ to } 10^5 \text{ KT} \qquad (3.14)$$

for an average 15-mph wind speed. For other average wind speeds, this distance on the pattern center line is calculated from

$$X_1 = X_2 - 0.174W^{0.337} \log I_{2,3} \text{ miles}; \quad W = 30 \text{ to } 10^5 \text{ KT} \qquad (3.15)$$

where X_2 and $I_{2,3}$ are given by Equation 3.1 and Equation 3.3, respectively.

The distances to locations between X_1 and X_2 for the intensity values, I_s, other than those of I_1 and $I_{2,3}$ are estimated from

$$X'_c = X_1 + \frac{(X_2 - X_1) \log I_s/I_1}{\log I_{2,3}/I_1} \qquad (3.16)$$

where X'_c is the distance from ground zero to the intensity value I_s along the center line of the pattern.

Because the upwind fallout intensity contour locations are based only on empirical data, the scaling system cannot be utilized to estimate the diameters of the particles landing at locations between X_1 and X_2.

3.2.4 Stem Pattern Half-Width

The (maximum) half-width of the stem fallout pattern, designated by Y_s, is the lateral distance from the center line of the stem pattern to the 1 R/hr at 1 hr contour; it is located at the downwind distance X_s given by

$$X_s = X_2 + \sqrt{(X_2 - X_1)^2 - Y_s^2}; \ (X_2 - X_1) > Y_s \qquad (3.17)$$

or

$$X_s = X_2; \ (X_2 - X_1) \le Y_s \qquad (3.18)$$

The value of $Y_s(15)$, for an average 15-mph wind speed is estimated from

$$Y_s(15) = 0.316W^{0.400} \text{ miles}; \ W = 1 \text{ to } 10^5 \text{ KT} \qquad (3.19)$$

For other wind speeds, the stem pattern half-width, $Y_s(v_w)$, is calculated from

13

$$Y_s(v_w) = Y_s(15)S_s(v_w) \qquad (3.20)$$

in which $S_s(v_w)$ is a wind velocity correction factor. The values of $S_s(v_w)$ are given as a function of weapon yield for several selected average wind speeds in Figure 3.2, the value of $S_s(v_w)$ for wind speeds other than those given in the figure can be obtained graphically from a linear plot of $S_s(v_w)$ against wind speed for a given weapon yield.

The lateral distances from the pattern center line to other intensity values between $I_{2,3}$ and the 1 R/hr at 1 hr contour (100 percent fission yield) at the downwind distance X_s are estimated from

$$Y_o^o = \frac{Y_s(v_w) \log (I_{2,3}/I_s)}{\log I_{2,3}/I_1} \qquad (3.21)$$

3.3 Fallout Deposition from Cloud Altitudes

3.3.1 Downwind Intensity Contours

The downwind intensity contour locations on the center line of the fallout pattern produced by particles falling from cloud heights are defined in terms of the intensities designated by I_5, I_6, I_7, and I_9 at the downwind distances X_5, X_6, X_7, and X_9, respectively, as shown in Figure 3.1.

The dimensions and height of the assumed elliptical source volume for the particles falling from the cloud starting at times of about 3 to 10 minutes after detonation, as derived from the data reported by Pugh and Galiano[12] and by Schuert,[5] are represented by the following yield-dependent functions:

$$r = 0.464W^{0.431} \text{ miles}; \quad W = 1 \text{ to } 10^5 \text{ KT} \qquad (3.22)$$

$$b = 0.265W^{0.300} \text{ miles}; \quad W = 1 \text{ to } 10^5 \text{ KT} \qquad (3.23)$$

$$h = 3.18W^{0.164} \text{ miles}; \quad W = 30 \text{ to } 10^5 \text{ KT} \qquad (3.24)$$

14
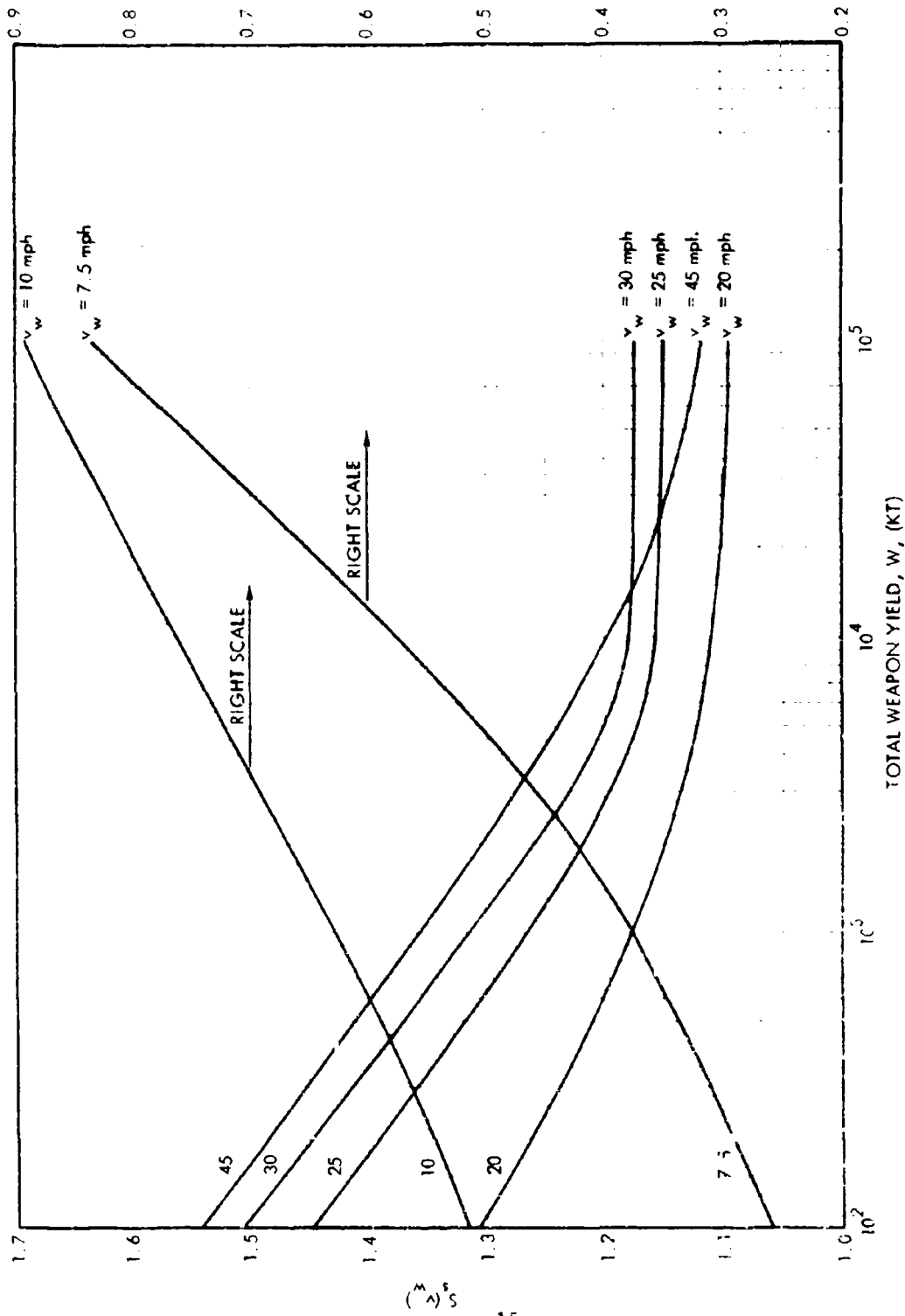
Fig. 3.2. Variation of the Stem Pattern Half-Width Wind Velocity Correction Factor with Weapon Yield for Several Average Wind Speeds

where r is the cloud radius, b is the cloud half-thickness, and h is the altitude of the center of the cloud. To a first approximation, r represents the cloud radius at the time the cloud top reaches its maximum height; the visible cloud radius continues to increase for some time thereafter.

In the fallout pattern scaling system, the variation of the downwind distance with weapon yield of the selected contour locations is mainly accounted for by setting the various characteristic distances proportional to the cloud height for a given average wind speed. For the locations under the cloud, some correction to allow for a decreased effective cloud radius is included in the scaling function. An additional, but smaller, dependence on weapon yield of the distances to the selected contour locations is included to account for a gradual shift in the radioactive content and in the average diameter of the particles that land at the designated locations. This change in radioactive content is apparently caused by a gradual increase in the proportion of the radioactive nuclides carried by the smaller particles as the weapon yield increases.

The scaling functions for estimating the distances and the intensities for the selected contour locations are given in two sets, depending on whether the downwind distance is less or greater than the cloud radius. For average wind speeds less than a given speed, the distances X_5 and X_6 are less than the cloud radius, r; the scaling functions for these distances and wind speed limits for a given weapon yield are given by

$$X_5 = 0.186W^{0.254}(v_w - 2.49W^{0.177}) \text{ miles; } v_w \leq 3.28W^{0.245} \text{ mi/hr;}$$

$$W = 30 \text{ to } 10^5 \text{ KT} \tag{3.25}$$

and

$$X_6 = 0.179W^{0.309}(v_w - 2.59W^{0.122}) \text{ miles; } v_w \leq 2.04W^{0.231} \text{ mi/hr;}$$

$$W = 30 \text{ to } 10^5 \text{ KT} \tag{3.26}$$

16

The downwind distances to all selected locations that are greater than cloud radius are represented by

$$X_i = v_w X_i^O W^{n_i} \text{ miles} \tag{3.27}$$

in which X_i^O and n_i are constants, and the subscript i represents one of the selected locations; derived values of X_i^O and n_i are summarized in Table 3.1.

The standard intensity for each of the selected locations is calculated from

$$I_i = K_i^O W^{m_i} \log \varphi_i(v_w) \text{ R/hr at 1 hr} \tag{3.28}$$

in which K_i^O and m_i are constants, and $\varphi_i(v_w)$ is given by

$$\varphi_i(v_w) = \frac{v_w + \sqrt{v_w^2 + 3.06 \, v_i^2(m)W^{0.262}}}{0.0531 \, v_i(m)W^{0.080}\left[v_w + \sqrt{v_w^2 + 1.085W^{0.102}}\right]};$$

$$v_w \leq v_i r/h \; ; \; W = 30 \text{ to } 10^5 \text{ KT} \tag{3.29}$$

or

$$\varphi_i(v_w) = \frac{(v_w + v_i r/h) + \sqrt{v_i^2 r^2 b^{-2} + (v_w + v_i r/h)^2}}{(v_w - v_i r/h) + \sqrt{v_i^2 r^2 b^{-2} + (v_w - v_i r/h)^2}};$$

$$v_w \leq v_i r/h \; ; \; W = 30 \text{ to } 10^5 \text{ KT} \tag{3.30}$$

in which v_i is the average value of the fall vector for the particles deposited at the location designated by i, and $v_i(m)$ is the minimum value of the fall vector of the deposited particles. The value of I_9 obtained from Equations 3.27 and 3.28 results in

17

Table 3.1

SUMMARY OF DOWNWIND DISTANCE AND STANDARD INTENSITY SCALING EQUATION CONSTANTS
FOR SELECTED LOCATIONS ON THE CLOUD FALLOUT PATTERN CENTER LINE[a]

i	x_i^o (mi)	n_i	K_i^o (R/hr at 1 hr)	m_i	v_i^o (mi/hr)	P_i	$(v_i r/h)_i^o$ (mi/hr)	q_i	$(v_i^2 r^2 b^{-2})_i^o$ (mi/hr)^2	r_i
5	0.142	0.186	14.57	-0.141	22.5	-0.022	3.28	0.245	1,550	0.218
			46.12[b]	-0.012[b]	17.1[b]	-0.090[b]	2.49[b]	0.177[b]	896[b]	0.082[b]
6	0.227	0.200	828.7	0.357	14.0	-0.036	2.04	0.231	601	0.190
			1,345[b]	0.393[b]	17.8[b]	-0.145[b]	2.59[b]	0.122[b]	971[b]	-0.028[b]
7	0.234	0.305	1,169	0.394	13.6	-0.141	1.98	0.126	565	-0.020
9[c]	2.027	0.310	-	-	1.57	-0.146	-	-	-	-

a For $W = 30$ to 10^5 KT; $v_w = 10$ to 50 mi/hr; the constants not defined in the text are for the following parameters:

$$v_i = v_i^o W^{P_i}$$

$$v_i r/h = (v_i r/h)_i^o W^{q_i}$$

$$v_i^2 r^2 b^{-2} = (v_i^2 r^2 b^{-2})_i^o W^{r_i}$$

b These values of the constants are for the condition where $v_w \leq v_i r/h$ (all other values apply to the condition of $v_w > v_i R/h$); the respective values of v_i^o and P_i are for the equation $v_i(m) = v_i^o W P_1$.

c $I_9 = 15/v_w$ r/hr at 1 hr for v_w in mi/hr.

$$I_9 = 15.0/v_w \qquad (3.31)$$

for v_w in miles per hour.

The empirically derived values for the constants of the intensity scaling functions for each of the selected contour locations are also summarized in Table 3.1. The median diameter of the particles deposited at each of the selected locations is estimated from the v_i values calculated from the functions of Table 3.1 (after multiplying by 1.467 to convert the values from mi/hr to ft/sec) using data given in Reference 4, along with h, the cloud center height, as the height of origin of the particle source.

One of the major characteristics of the fallout pattern scaling system for the fallout from the cloud altitudes is that it specifies a peak in the downwind intensity profile at X_7. The intensity, I_7, gradually increases with weapon yield approximately proportional to $W^{0.4}$. No experimental data are available for testing the reliability of the estimates of I_7 obtained from extrapolation of the scaling functions to very high weapon yields.

The downwind distances to contours of other standard intensities on the cloud fallout pattern center line are estimated from

$$X'_c = X_5 + \frac{(X_6 - X_5) \log (I_s/I_5)}{\log (I_6/I_5)}; \quad I_s \le I_6 \qquad (3.32)$$

$$X'_c = X_6 + \frac{(X_7 - X_6) \log (I_s/I_6)}{\log (I_7/I_6)}; \quad I_6 \le I_s \le I_7 \qquad (3.33)$$

or

$$X_c = X_7 + \frac{(X_9 - X_7) \log (I_7/I_s)}{\log (I_7/I_9)}; \quad I_s \le I_7 \qquad (3.34)$$

where X'_c is the downwind distance to the intensity, I_s, for the distances less than X_7, and X_c is the distance to the intensity, I_s, for distances beyond X_7.

19

3.3.2 Maximum Pattern Half-Width

The maximum pattern half-width for fallout from cloud altitudes is designated as Y_8, and the downwind distance to Y_8 is designated as X_8 (see Figure 3.1). The empirically derived scaling function for X_8 is given by

$$X_8 = 0.325 v_w W^{0.315} \text{ miles}; \ W = 30 \text{ to } 10^5 \text{ KT} \tag{3.35}$$

The crosswind distances to given contours in the fallout area depend, first, on the lateral displacement of the particles during the rise of the cloud; second, on the wind directions at all altitudes from the bottom to the top of the cloud; and third, on the wind speeds.

The wind speed has two effects on the lateral displacement of an intensity contour. One is the horizontal displacement of particles with wind speed because of the relative horizontal distance traveled in a given period of time. The other is the decrease in surface density of a given size group with wind speed because of the change in the angle of the particle trajectory. Hence, even for the case in which the wind direction is the same at all altitudes, a change in wind speed results in a change in the maximum crosswind distance of a given intensity contour.

The values of $Y_8^o(15)$ for the maximum lateral distance from the pattern center line to the 1 R/hr at 1 hr contour for an average wind speed of 15 miles per hour, as derived from both observed data and summations of the fraction of the radioactivity contained in the fallout pattern (see Section 3.4), are summarized in Table 3.2. The computed pattern widths include the effect of lateral wind shear contained in the original data; this effect is discussed in Paragraph 3.5.4. Approximate scaling functions for $Y_8^o(15)$ are as follows:

$$Y_8^o(15) \simeq 0.518 W^{0.615} \text{ miles}; \ W = 30 \text{ to } 750 \text{ KT} \tag{3.36}$$

20

Table 3.2

SUMMARY OF CALCULATED $Y^O_8(15)$ VALUES FOR SELECTED WEAPON YIELDS[a]

W (KT)	$Y^O_8(15)$ (miles)	W (MT)	$Y^O_8(15)$ (miles)
5	1.90	1	33.6
10	2.28	2	40.9
20	3.18	5	53.4
50	5.76	10	64.7
100	9.10	20	78.0
200	14.0	50	101
500	23.5	100	123

a   For 100 percent fission yield

and

$$Y^O_8(15) \simeq 4.75W^{0.283} \text{ miles; } W = 750 \text{ to } 10^5 \text{ KT} \tag{3.37}$$

The variation of Y_8 with wind speed (for a given wind direction) is determined relative to $Y^O_8(15)$ for a wind speed of 15 miles per hour. The representation for the variation is

$$Y_8(v_w) = Y^O_8(15)S(v_w) \tag{3.38}$$

in which $S(v_w)$ is the relative shear factor due to wind speed only.

The values of $S(v_w)$ determined from the fallout scaling system parameters for different wind speeds are essentially independent of weapon yield. The indicated value of $Y_8(v_w)$ is for the particle groups falling at the downwind distance, X_8; the associated intensity contour that passes through the location of $Y_8(v_w)$, X_8, is equal to I_9 for the same wind speed. The intensity at the location is thus 1 R/hr at 1 hr when the wind speed is 15 miles per hour. Values of $S(v_w)$ at several wind speeds, and the associated intensities, are given in Table 3.3; the tabulated values of $S(v_w)$ are represented approximately by

$$S(v_w) \simeq 0.360(1 + 26.7/v_w); \quad v_w = 10 \text{ to } 22.6 \text{ mi/hr} \tag{3.39}$$

and

$$S(v_w) \simeq 0.426(1 + 19.0/v_w); \quad v_w = 22.6 \text{ to } 50 \text{ mi/hr} \tag{3.40}$$

Combining Equations 3.39 and 3.40 with Equations 3.36 and 3.37 gives, for $Y_8(v_w)$,

$$Y_8(v_w) \simeq 0.186W^{0.615} (1 + 26.7/v_w) \text{ miles; } v_w = 10 \text{ to } 22.6 \text{ mi/hr} \tag{3.41}$$

$$Y_8(v_w) \simeq 0.221W^{0.615} (1 + 19.0/v_w) \text{ miles; } v_w = 22.6 \text{ to } 50 \text{ mi/hr} \tag{3.42}$$

22

Table 3.3

SUMMARY OF THE RELATIVE WIND SPEED SHEAR FACTOR, $S(v_w)$,
FOR THE FALLOUT PATTERN MAXIMUM HALF-WIDTH AND
ASSOCIATED STANDARD IONIZATION RATE
FOR SEVERAL WIND SPEEDS

Wind Speed (mi/hr)	$S(v_w)$	I_9 (R/hr at 1 hr)
10	1.325	1.5
15	1.000	1.0
20	0.840	0.75
25	0.750	0.60
30	0.695	0.50
35	0.658	0.428
40	0.630	0.375
45	0.605	0.333

for W values between 30 and 750 KT; and

$$Y_8(v_w) \simeq 1.71 W^{0.283} (1 + 26.7/v_w) \text{ miles}; \quad v_w = 10 \text{ to } 22.6 \text{ mi/hr} \qquad (3.43)$$

$$Y_8(v_w) \simeq 2.02 W^{0.283} (1 + 19.0/v_w) \text{ miles}; \quad v_w = 22.6 \text{ to } 50 \text{ mi/hr} \qquad (3.44)$$

for W values between 750 and 10^5 KT.

The value of Y_8^o for the 1 R/hr at 1 hr contour for a given wind speed (100 percent fission yield) is estimated from

$$Y_8^o(1) = \frac{Y_8(v_w) \log I_7}{\log (I_7/I_9)} \qquad (3.45)$$

where I_7 and I_9 are the intensities at X_7 and X_9 (Y = 0) for a given value of v_w.

The maximum lateral distance to other intensity values between I_7 and the 1 R/hr at 1 hr contour at X_8, $Y_8^o(1)$ is estimated from

$$Y_8(I) = Y_8^o(1) \frac{\log (I_7/I_s)}{\log I_7} \qquad (3.46)$$

The downwind distance to $Y_8(I)$ is given by

$$X_8(I) = X_7 + \frac{(X_8 - X_7) \log (I_7/I_s)}{\log (I_7/I_9)} \qquad (3.47)$$

3.4 Idealized Fallout Pattern Shapes and Areas Within Contours

3.4.1 Stem Pattern Contours

With the simplified fallout scaling system and the stylized downwind intensity profile, it is convenient to construct contours by using simple geometric forms which approximate to some degree the true shapes of the contours

24

and, within reasonable limits, account for the fraction of the activity produced that falls back to earth within their areas.

The assumed shape of the intensity contours for the fallout from stem altitudes is a combination of a half-ellipse and a partial circle having its center at X_2, providing the distance $(X_2 - X_c')$ is equal to or larger than the distance Y_o^o for the same contour of the stem pattern. For these conditions, the major axis of the half-ellipse on the center line in the downwind direction is $(X_c - x_s)$ where x_s is equal to $X_2 + [(X_2 - Y_c')^2 - Y_o^o{}^2]^{1/2}$ and the minor axis is Y_o^o the ellipse is centered at x_s on the pattern center line.

The equations for the assumed intensity contour shapes, accordingly, are given by

$$(X - X_2)^2 + Y^2 = (X_2 - X_c')^2; \quad X = -X_c' \text{ to } x_s \tag{3.48}$$

and

$$\frac{(X - x_s)^2}{(X_c - x_s)^2} + \frac{Y^2}{(Y_o^o)^2} = 1; \quad X = x_s \text{ to } X_c \tag{3.49}$$

The area contained within a given standard intensity contour, for the above assumed contour geometry, is given by

$$a_s = 3.1416(X_2 - X_c')^2 \left[1 - \frac{\sin^{-1}\left[Y_o^o/(X_2 - X_c')\right]}{180} \right] + 1.5708Y\left[X_c - X_2\right]$$

$$- 0.5708Y\sqrt{(X_2 - X_c')^2 - Y_o^2}; \quad (X_2 - X_c') \geq Y_o^o \tag{3.50}$$

or

$$a_s = \frac{\log\,(I_{2,3}/I_s)}{\log\,I_{2,3}}\left[\left\{\frac{3.1416(X_2 - X_1)^2}{\log\,I_{2,3}}\left[1 - \frac{\sin^{-1}Y_s(v_w)/(X_2 - X_1)}{180}\right]\right.\right.$$

$$+ \frac{1.5708Y_s(v_w)(X_4 - X_3)}{\log\,(I_{2,3}/I_4)} - \frac{0.5708Y_s(v_w)}{\log\,I_{2,3}}\sqrt{(X_2 - X_1)^2 - Y_s^2(v_w)}\left.\right\}\log\,(I_{2,3}/I_s)$$

$$\left.+ 1.5708Y_s(v_w)(X_3 - X_2)\right]; \quad (X_2 - X_1) \geq Y_s(v_w) \tag{3.51}$$

The total activity contained within the stem fallout pattern, obtained from the integration of $I_s\,da_s$ (where da_s is calculated from Equation 3.51 over the intensity limits from $I_{2,3}$ to I_4, is given by

$$A_s = \frac{I_{2,3}}{\log\,I_{2,3}}\left\{\frac{1.186(X_2 - X_1)^2}{\log\,I_{2,3}}\left[1 - \frac{\sin^{-1}Y_s(v_w)/(X_2 - X_1)}{180}\right]\right.$$

$$+ \frac{0.593Y_s(v_w)(X_4 - X_3)}{\log\,(I_{2,3}/I_4)} - \frac{0.2154Y_s(v_w)\sqrt{(X_2 - X_1)^2 - Y_s^2(v_w)}}{\log\,I_{2,3}}$$

$$\left.+ 0.682Y_s(v_w)(X_3 - X_2)\right\}; \quad (X_2 - X_1) \geq Y_s(v_w); \quad I_{2,3} \gg I_4 \tag{3.52}$$

For some conditions of wind speed and weapon yield, the maximum half-width distance, Y_o^o, will exceed the distance $(X_2 - X_c')$. As an example, $Y_s(v_w)$ for the 1 R/hr at 1 hr contour exceeds the distance $(X_2 - X_1)$ for weapon yields larger than 22 MT and a 15 mile per hour wind speed. The assumed contour shape for the case where $Y_o^o \geq (X_2 - X_c')$ is that of two half-ellipses, both centered at the point X_2 on the pattern center line. The upwind half-ellipse has a major axis given by Y_o^o and a minor axis given by

26

$(X_2 - X_c')$; the downwind half-ellipse has a major axis given by $(X_c - X_2)$ and a minor axis given by Y_o^o. The general equations for the idealized intensity contour shapes are

$$\frac{(X_2 - X)^2}{(X_2 - X_c')^2} + \frac{Y^2}{(Y_o^o)^2} = 1; \quad X \le X_2 \tag{3.53}$$

and

$$\frac{(X - X_2)^2}{(X_c - X_2)^2} + \frac{Y^2}{(Y_o^o)^2} = 1; \quad X \ge X_2 \tag{3.54}$$

The area contained within a given standard intensity contour, for the two half-ellipses, is

$$a_s = 1.5708Y(X_c - X_c'); \quad Y_o^o \ge (X_2 - X_c') \tag{3.55}$$

or

$$a_s = \frac{1.5708Y_s(v_w) \log (I_{2,3}/I_s)}{\log I_{2,3}} \left\{ \left[\frac{(X_2 - X_1)}{\log I_{2,3}} + \frac{(X_4 - X_3)}{\log (I_{2,3}/I_4)} \right] \log (I_{2,3}/1_s) \right.$$
$$\left. + (X_3 - X_2) \right\}; \quad Y_s(v_w) \ge (X_2 - X_1) \tag{3.56}$$

The total activity contained within these contour areas is given by

$$A_s = \frac{0.682Y_s(v_w)I_{2,3}}{\log I_{2,3}} \left\{ 0.858 \frac{(X_2 - X_1)}{\log I_{2,3}} + \frac{(X_4 - X_3)}{\log (I_{2,3}/I_4)} \right\} + (X_3 - X_2);$$
$$Y_s(v_w) \ge (X_2 - X_1); \quad I_{2,3} \gg I_4 \tag{3.57}$$

27

3.4.2 Cloud Pattern Contours

The assumed shape of the intensity contours for the fallout pattern formed by particles falling from cloud altitudes is described by two half-ellipses smoothly joined at the downwind distance of the maximum width of the contour. The locations of the maximum contour widths fall on a line joining X_7 on the pattern center line $(Y = 0)$ and the point $X_8(I), Y_8(I)$ (see Equations 3.46 and 3.47).

The general equations for this idealized contour shape are

$$\frac{[X_8(I) - X]^2}{[X_8(I) - X_c']^2} + \frac{Y^2}{Y_8^2(I)} = 1; \quad X \leq X_8(I) \tag{3.58}$$

and

$$\frac{[X - X_8(I)]^2}{[X_c - X_8(I)]^2} + \frac{Y^2}{Y_8^2(I)} = 1; \quad X \geq X_8(I) \tag{3.59}$$

The area contained with a given standard intensity contour is given by

$$a_c = 1.5708 Y_8 (X_c - X_c') \tag{3.60}$$

in terms of the designated distances; in terms of intensities and scaled pattern features, the areas within contours are given by

$$a_c = \frac{1.5708 Y_8 (v_w) \log(I_7/I_s)}{\log (I_7/I_9)} \left[\frac{(X_9 - X_7) \log(I_7/I_s)}{\log (I_7/I_9)} - \frac{(X_7 - X_6) \log(I_s/I_6)}{\log (I_6/I_5)} \right.$$
$$\left. + (X_7 - X_5) \right]; \quad I_s \leq I_6 \tag{3.61}$$

and

$$a_c = \frac{1.5708Y_8(v_w)\log(I_7/I_s)}{\log(I_7/I_9)}\left[\frac{(X_9 - X_7)\log(I_7/I_s)}{\log(I_7/I_9)} - \frac{(X_7 - X_\cdots)\log(I_s/I_6)}{\log(I_7/I_9)}\right.$$

$$\left. + (X_7 - X_6)\right] ; \quad I_6 \leq I_s \leq I_7 \tag{3.62}$$

The activity integral for the cloud fallout pattern, designated A_c, can be estimated from

$$A_c = \frac{1.364Y_8(v_w)}{\log I_7}\left\{\frac{(X_9 - X_7)}{\log(I_7/I_9)} + \frac{(X_7 - X_6)}{\log(I_7/I_6)}\right\}\left\{0.434(I_7 - I_6) - I_6\log(I_7/I_6)\right\}$$

$$+ \frac{0.6822Y_8(v_w)I_6}{\log I_7}\left\{\frac{(X_9 - X_7)}{\log(I_7/I_9)}\left[2\log(I_7/I_6) + 0.868\right]\right.$$

$$+ \frac{(X_6 - X_5)}{\log(I_6/I_5)}\left[\log(I_7/I_6) - \log(I_6/I_5) + 0.868\right] + X_7 - X_5\right\} \tag{3.63}$$

for the case where $I_6 \gg I_s$.

3.4.3 Summary of Pattern Features and Activity Summations

The fission-product radioactivity produced by a detonation is about 1.4×10^{23} BW fissions where W is the total yield in KT and B is the ratio of fission to total yield. Some fraction of this total activity is contained within the fallout pattern. If the activity in a pattern is summed over the fallout area from the central high intensities down to a stated low-valued intensity contour enclosing the largest area, the fraction accounted for increases with yield. An ionization rate or intensity sum of a fallout pattern made in this way does not account for the activity deposited on the ground at

29

lower intensities than the selected "lowest" contour, nor does it account for the fraction carried away on very small particles as world-wide fallout. The sum or integration of the activity over the fallout area can be used, however, to determine the fraction of the activity that is accounted for in the fallout pattern out to a stated low-level contour; the equations of such a summation for the simplified fallout scaling system are given in the two preceding sections.

The amount of activity accounted for in a fallout pattern is defined by

$$C(1)\overline{K(1)} \; 1.4 \times 10^{23} \mathrm{BW} = \int_0^{a_o} I_s \, da \tag{3.64}$$

in which $C(1)$ is the true fraction of the number of fissions accounted for, and $\overline{K(1)}$ is the average value of the ratio of R/hr at 1 hr to the number of fissions or kiloton equivalents per unit area for all the activity within the area, a_o. The average or accumulated fractionation number, for the radioactive elements accounted for, may be defined through $\overline{K(1)}$ by

$$\overline{K(1)} = \delta\bar{q} \left[\overline{r_{fp}(1)} \; i_{fp}(1) + i_i(1) \right] \tag{3.65}$$

in which δ is an instrument response factor, $\bar{q}$ is a terrain attenuation factor, $\overline{r_{fp}(1)}$ is an average gross fractionation number for the fission products applicable to the ionization rates at H + 1, $i_{fp}(1)$ is the H + 1 air ionization rate at 3 ft above an infinite ideal plane for a unit surface density of unfractionated fission products spread over the plane, and $i_i(1)$ is in the same units for neutron-induced activities. The units of measure for $\overline{K(1)}$ are the same as for $i_{fp}(1)$ and $i_i(1)$ and usually are given in terms of either R/hr at 1 hr per fission/sq ft or R/hr at 1 hr per KT/sq mi. It may be noted that the true air ionization rate is obtained when the value of δ is set equal to one.

30

The empirical constants for the scaling functions of the simplified fallout scaling system apply to the reference condition of 100 percent fission yield (B = 1), including 0.8 neutron captures per fission by U-238 to give the appropriate value of I_s in R/hr at 1 hr.

Also, the I_s values (or standard intensities) correspond to radiac measurements taken at 3 ft above an extended open area contaminated with fallout as it existed when the measurements were taken. The reference radiac instrument for the I_s values is the AN/PDR-39(T1B) portable radiac; it has a geometric and photon energy response at very nearly 75 percent of the true air ionization rate at 3 ft above a plane source of fission products uniformly distributed on the area. Therefore to obtain the true air ionization, in calculating exposure doses, the I_s values should be multiplied by 1.33.

The average value of the terrain shielding factor, which is automatically contained in the source data, is about 0.75. The data, in general, apply to U-238 fission, for which the $i_{fp}(1)$ of Equation 3.65 is equal to 6.94×10^{-13} R/hr at 1 hr per fission/sq ft or 3,510 R/hr at 1 hr per KT/sq mi. The value of $i_i(1)$ for the indicated induced activities is 0.13×10^{-13} R/hr at 1 hr per fission/sq ft. With these numbers, Equation 3.65 becomes

$$\overline{K(1)} = 3.90 \times 10^{-13} \left[\overline{r(1)} + 0.019 \right] \frac{\text{R/hr at 1 hr}}{\text{fission/sq ft}} \tag{3.66}$$

or

$$\overline{K(1)} = 1,970 \left[\overline{r(1)} + 0.019 \right] \frac{\text{R/hr at 1 hr}}{\text{KT/sq mi}} \tag{3.67}$$

With Equation 3.67, the intensity-area integral becomes

$$\int_0^{a_0} I_s da = 1,970 \left[\overline{r(1)} + 0.019 \right] C(1)BW \tag{3.68}$$

It can be seen that, for unfractionated fission products $(\overline{r(1)} = 1)$ and for C(1) equal to unity, the ideal or upper limit value of the intensity-area integral per unit yield would be about 2,010 R/hr at 1 hr for observed fallout pattern intensities.

31

Values of the various fallout pattern features from the various scaling
functions and intensity-area integral parameters are summarized in Table 3.4
for selected weapon yields. The area integrals indicate that the fraction of
the total activity contained within the 1 R/hr at 1 hr contour for the simpli-
fied fallout pattern scaling systems varies from about 0.4 for a weapon yield
of 1 KT to about 0.8 for a weapon yield of 100 MT. Although the scaling
functions given in the previous sections apply only to weapon yields in the
range of 30 KT to 100 MT (for the latter high yield as an extrapolation),
tabulated values for 1 and 10 KT are included in Table 3.4 as derived from
the data of Reference 4.

3.5 Ionization Rates and Potential Exposure Doses During Fallout Arrival

3.5.1 Times of Fallout Arrival and Cessation

The arrival time of fallout particles from stem altitudes is
estimated as the sum of two time periods. The first of these is the time
required for the particles of a given average fall velocity to pass through
the fireball and circulate in a toroidal motion until the updraft from the
buoyant gases no longer carry the particles upward; the second time period
is that of gravity fall under influence of winds to the ground.

The apparent height at which particles of different diameters (and given
fall velocities) are effectively free of the updraft under the rising fireball
and cloud is estimated from

$$Z_f = 1.80 \times 10^4 W^{0.116} \left[1 - \exp (-0.00599 W^{-0.116} t) \right] \text{ ft};$$

$$t \geq 20 \text{ sec}; W = 30 \text{ to } 10^5 \text{ KT} \tag{3.69}$$

The rate of increase of the apparent height with time after detonation at
which the particles assume free fall is then given by

Table 3.4

SUMMARY OF FALLOUT PATTERN FEATURES AND FALLOUT SCALING SYSTEM PARAMETER VALUES FOR AN ASSUMED EFFECTIVE WIND SPEED OF 15 MPH[a]

Pattern Feature or Quantity	Weapon Yield					
	1 KT	10 KT	100 KT	1 MT	10 MT	100 MT
X_1	-0.385	-1.21	-3.01	-6.29	-13.1	-27.3
X_2	0.0648	0.342	0.735	0.882	0.574	-1.02
X_3	0.352	0.967	2.06	4.00	7.68	14.7
X_4	1.46	5.18	12.1	19.3	30.8	48.6
X_5	0.834	2.58	5.00	7.03	4.39	-14.3
X_6	1.34	4.05	8.56	13.6	21.6	27.9
X_7	1.38	5.30	14.4	28.8	58.4	118
X_8	1.91	7.56	20.8	42.8	88.6	183
X_9	29.4	61.2	126	258	528	1,080
$Y_s(15)$	0.316	0.796	1.99	5.02	12.6	31.6
$Y_8^o(15)$	1.26	2.28	9.10	33.6	64.7	123
$I_{2,3}$	1,730	22,900	35,300	9,800	3,550	1,440
I_6	130	222	540	1,720	5,270	15,500
I_7	180	317	803	2,712	9,070	30,510
A_s/W^b	93.4	724	544	77.5	14.4	3.3
A_c/W^b	757	416	687	1,250	1,412	1,552
A_T/W^b	850	1,140	1,231	1,328	1,426	1,555
$\overline{(r(1)} + 0.019)^c$	0.785	0.787	0.789	0.793	0.797	0.803
$C(1)$	0.550	0.735	0.792	0.850	0.908	0.983
$z_{2,3}^d$	3,430	8,910	15,800	22,900	32,300	44,400
z_o^d	5,200	15,600	30,800	40,200	52,500	68,500
h^d	6,600	18,400	35,700	52,300	76,200	111,000

a Distances are in miles; intensities are in R/hr at 1 hr (observed); reference: 100 percent fission yield

b In R/hr at 1 hr per KT/sq mi; integrated to the 1 R/hr at 1 hr contour

c $\overline{r(1)}$ calculated from data of Chapter 4

d Altitudes in feet

$$\dot{Z}_f = 108 \exp (-0.00599W^{-0.116}t) \text{ ft/sec}; \quad t \geq 20 \text{ sec};$$

$$W = 30 \text{ to } 10^5 \text{ KT} \tag{3.70}$$

Approximate representations of the relationships between the particle fall rate, $\dot{Z}_f$, at the height Z and the particle fall velocity vector, v_f, for a particle falling from the height Z to the ground (sea level) were derived for spherical particles from particle fall rate data as computed by Cassidy[15]; these are:

$$\dot{Z}_f/v_f = 1.00 + 2.00 \times 10^{-6}Z_f; \quad v_f < 2.0 \text{ ft/sec}; \quad Z = 0 \text{ to } 10^5 \text{ ft} \tag{3.71}$$

$$\dot{Z}_f/v_f = 0.948 - 0.0530 \log v_f + 3.78 \times 10^{-6}(1.259 + \log v_f)Z_f;$$

$$v_f = 2.0 \text{ to } 200 \text{ ft/sec}; \quad Z = 10^4 \text{ to } 6 \times 10^4 \text{ ft} \tag{3.72}$$

The relationship among $\dot{Z}_f$, v_f, and Z_f given by Equation 3.72 represents the tabulated data within 10 percent at the extremes of the indicated limits of application for v_f and Z. The indicated ranges in these parameters include all the values applicable to the fallout from the stem heights of interest; therefore, Equation 3.72 generally is used, along with Equations 3.69 and 3.70, to estimate the time after detonation when particles with a given fall vector leave the rising cloud and take on free fall. This time is given by

$$t_1 = 0.107W^{0.116} \left\{ \log\left[1585/v_f + (1.259 + \log v_f) \, W^{0.116} \right] \right.$$

$$\left. - \log\left[0.779(17.887 - \log v_f) + (1.259 + \log v_f) \, W^{0.116} \right] \right\} \text{hr} \tag{3.73}$$

The time for the particles with a given value of v_f to fall from the height Z_f ($Z_f \leq 60,000$ ft) is estimated from

$$t_2 = \frac{3.895 \left[2,034/v_f + \log v_f - 17.887\right]}{\left[1,585W^{-0.116} + v_f (1.259 + \log v_f)\right]} \text{ hr} \tag{3.74}$$

Equations 3.73 and 3.74 apply to v_f values between 2 and 200 ft/sec and to W values between 30 and 10^5 KT. With Equation 3.71, the times are

$$t_1 = 0.107W^{0.116} \left[\log (27.78 + W^{0.116}) - \log (2,995/v_f + W^{0.116})\right] \text{ hr} \tag{3.75}$$

and

$$t_2 = \frac{277.8 \left[108 - v_f\right]}{v_f \left[2.0 \, v_f + 5,990W^{-0.116}\right]} \text{ hr} \tag{3.76}$$

for v_f values less than 2 ft/sec and W values between 30 and 10^5 KT.

The time of arrival on the ground, t_a, for the particles with the falling velocity v_f is equal to $t_1 + t_2$.

The particles that reach the earth's surface first are those with the falling velocity, $v_{f_{2,3}}$. For these particles the times after detonation of leaving the cloud and of fall from Z_f to the ground are given by

$$t_1^o = 0.107W^{0.116} \left\{\log \left[290.1W^{0.080} + (38.66 - \log W)W^{0.116}\right]\right.$$

$$\left. - \log \left[0.779 (200.7 + \log W) + (38.66 - \log W)W^{0.116}\right]\right\} \text{ hr};$$

$$W = 30 \text{ to } 10^5 \text{ KT} \tag{3.77}$$

and

$$t_2^o = 0.0570W^{0.080} \frac{\left[372.2W^{0.080} - 200.7 - \log W\right]}{\left[290.1W^{-0.036} + 38.66 - \log W\right]} \text{ hr}; \quad W = 30 \text{ to } 10^5 \text{ KT} \tag{3.78}$$

Values of the earliest fallout arrival on the ground from stem heights as calculated from Equations 3.77 and 3.78, are given in Table 3.5 for several weapon yields.

The calculation of the time of fallout arrival and of fallout cessation (and the time period of deposition) for a given location on the stem fallout pattern center line requires estimates of the minimum and maximum values of v_f that arrive at the location. These two values of v_f are for the particles that fall from the upwind and downwind sides of the stem volume; they are determined from the stem radius and various relationships between the downwind distance, X, the fall vector, v_f, and the apparent height, Z_f, at which the particles take on free fall.

Table 3.5

ESTIMATED TIMES OF EARLIEST FALLOUT ARRIVAL FROM STEM ALTITUDES

W (KT)	t_1^o (hr)	t_2^o (hr)	t_a^o (hr)	t_a^o (min)
10^2	0.062	0.098	0.160	10
10^3	0.093	0.167	0.260	16
10^4	0.135	0.280	0.415	25
10^5	0.192	0.463	0.655	39

The maximum and minimum downwind distances of deposition along the center line of the stem fallout pattern for the particles that fall freely from the height, Z_f, are estimated from

$$X = 2.78 \times 10^4 (v_w/v_f)Z_f \pm 0.0395W^{0.333} \exp\left(1.48 \times 10^{-4}W^{-0.131}Z_f\right) \text{ miles};$$

$$W = 30 \text{ to } 10^5 \text{ KT} \tag{3.79}$$

where v_w is in mi/hr; v_f is in ft/sec; and Z_f is in feet. The value of Z_f for a selected value of v_f is estimated from

$$Z_f = \frac{10^6(108 - v_f)}{\left(2.0v_f + 5,990W^{-0.116}\right)} \text{ ft; } v_f < 2 \text{ ft/sec; } W = 30 \text{ to } 10^5 \text{ KT} \tag{3.80}$$

36

or

$$Z_f = \frac{1.40 \times 10^4 \left[2{,}034 - (17.887 - \log v_f)v_f \right]}{\left[(1.259 + \log v_f)v_f + 1{,}585W^{-0.116} \right]} \text{ ft};$$

$$v_f = 2 \text{ to } 200 \text{ ft/sec}; \quad W = 30 \text{ to } 10^5 \text{ KT} \tag{3.81}$$

The minimum and maximum values of v_f are determined by selecting a series of values of v_f starting with $v_f(2,3)$ as the largest value and then computing Z_f and the two values of X in Equation 3.79; the v_f values are plotted as a function of X to determine the paired values of v_f at a given value of X. Such a plot is shown in Figure 3.3 for the fallout from stem heights of a 5-MT yield detonation. The time of arrival of the particles with v_f values from the minimum to the maximum, for a given value of X, is computed by substituting selected values of v_f in Equations 3.73 and 3.74 or Equations 3.75 and 3.76 and solving for both t_1 and t_2.

Estimates of the v_f values and arrival times of the particles deposited at locations which are a distance of Y miles from the center line of the stem fallout pattern can be made by replacing the second term of Equation 3.79 with

$$\pm \left[1.56 \times 10^{-3} W^{0.667} \exp \left(2.96 \times 10^{-4} W^{-0.131} Z_f \right) - Y^2 \right]^{1/2} \tag{3.82}$$

The particles falling from cloud altitudes, the time of arrival on the ground of particles with the falling velocity, v_f, may be generally represented by

$$t_a = 0.17W^{-0.1} + t_f \quad \text{hr} \tag{3.83}$$

where $0.17W^{-0.1}$ hr is the apparent time to cloud stabilization and t_f is the time of fall from the height Z. The application of Equation 3.83 is discussed below in relation to: (1) the estimation of the time of arrival and cessation
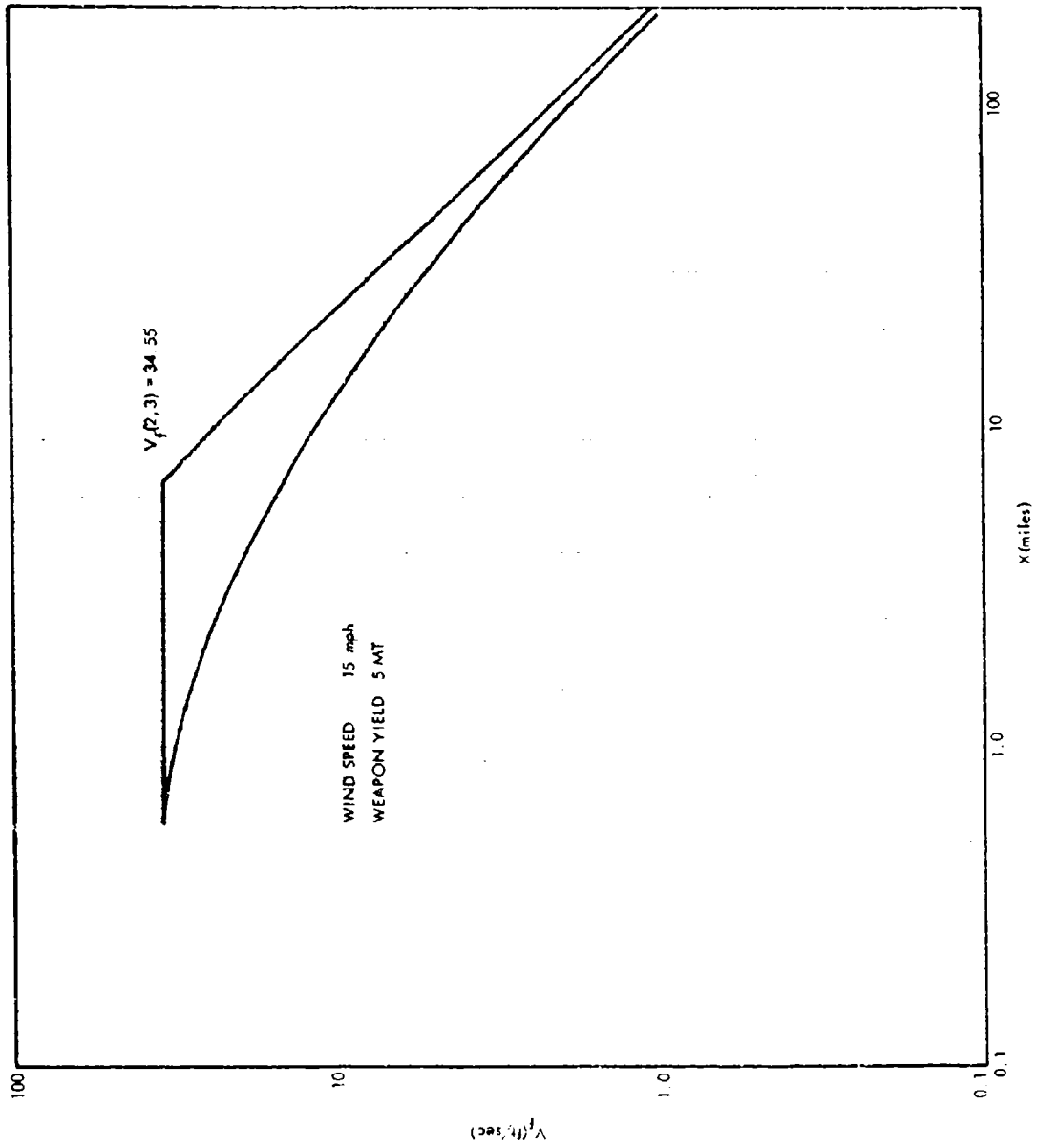
Fig. 3.3. Variation of the Computed Minimum and Maximum Values of v_f with Downwind Distance (center line of stem pattern) for Particles Falling from Stem Altitudes

of fallout at a given coordinate point, X, Y, with an assumed reference pattern spread due to lateral wind shear; (2) the estimation of the range in falling speeds (and diameters) of particles that arrive at a given location (as needed for estimating the gross activity-particle size distribution); and (3) the estimation of the influence of lateral wind shear at the cloud heights on the spread of the fallout pattern. In all treatments, it is assumed that the cloud radius, r, remains constant in the direction of the wind (i.e., the continuing lateral expansion of the cloud after $0.17W^{-0.1}$ hr is neglected).

The earliest arrival time of particles falling from the so-called stabilized cloud is that of the largest particles, with a fall vector designated by v_5, from the lower surface of the cloud. The general area on which these particles fall is defined by an ellipse whose axis on the center line of the pattern is equal to r and whose axis in the cross-wind direction is equal to a distance designated as Y_o. The first arrival time at downwind locations outside this elliptically shaped area of particles with falling speeds less than v_f is for the particles falling from the forward edge of the cloud (at the cloud center height, h). The general equation for t_f of the particles falling from the lower surface of the cloud that land at the point X, Y, is

$$t_f = \frac{\left(v_f h r^2 b^{-2} + v_w X\right) - r\sqrt{\left(v_f^2 r^2 b^{-2} + v_w^2\right)\left(1 - Y^2/Y_o^2\right) - \left(v_f h^{-1} X - v_w\right)^2 h^2 b^{-2}}}{\left(v_f^2 r^2 b^{-2} + v_w^2\right)} \text{ hr} \quad (3.84)$$

in which

$$hr^2 b^{-2} = 9.75 W^{0.426} \text{ mi}; \quad W = 30 \text{ to } 10^5 \text{ KT}$$

$$r = 0.464 W^{0.431} \text{ mi}; \quad W = 1 \text{ to } 10^5 \text{ KT}$$

$$r^2 b^{-2} = 3.07 W^{-0.262} \text{ mi}; \quad W = 1 \text{ to } 10^5 \text{ KT}$$

$$h^{-1} = 0.314 W^{-0.164} \text{ mi}^{-1}; \quad W = 30 \text{ to } 10^5 \text{ KT}$$

$$h^2 b^{-2} = 144 W^{-0.272}; \quad W = 30 \text{ to } 10^5 \text{ KT}$$

for v_w and v_f in mi/hr.

The assumed equation for Y_o, the peripheral limit of the fallout pattern in the cross-wind direction is

$$Y_o = 2Y_8(v_w) \left[1 - e^{-k_c(X_c + r)}\right] \text{miles} \qquad (3.85)$$

where $Y_8(v_w)$ is given by Equations 3.41 through 3.44; this form of representation assumes persistence of lateral shear such that the pattern spread at very large downwind distances is twice the width, $Y_8(v_w)$, at the downwind distance, X_8. Further, it is assumed that Y_o is equal to 1.1 $Y_8(v_w)$ at X_8 so that

$$k_c = 0.8/(X_8 + r) \text{ miles}^{-1} \qquad (3.86)$$

or

$$k_c = \frac{2.46W^{-0.315}}{\left(v_w + 1.395W^{0.116}\right)} \text{ miles}^{-1} \qquad (3.87)$$

Substitution of v_5 from Table 3.1 for v_f in Equation 3.84 gives

$$t_f = \frac{\left(219W^{0.404} + v_w X\right)}{1.550W^{0.218} + v_w^2} -$$

$$\frac{0.464W^{0.431} \sqrt{\left(1,550W^{0.218} + v_w^2\right)\left(1 - Y^2/Y_o^2\right) - 144\left(7.08 \times W^{-0.186} - v_w\right)^2 W^{-0.272}}}{1,550W^{0.218} + v_w^2}$$

$$\text{hrs; } v_w \geq 3.82W^{0.245}; \ W = 30 \text{ to } 10^5 \text{ KT} \qquad (3.88)$$

40

or

$$t_f = \frac{\left(167W^{0.336} + v_w X\right)}{896W^{0.082} + v_w^2} -$$

$$\frac{0.464W^{0.431}\sqrt{\left(896W^{0.082} + v_w^2\right)\left(1 - Y^2/Y_o^2\right) - 144\left(5.38 \ X \ W^{-0.254} - v_w\right)^2 W^{-0.272}}}{896W^{0.082} + v_w^2}$$

hrs; $v_w < 3.28W^{0.245}$; $W = 30$ to 10^5 KT (3.89)

The approximate limits of X on the pattern center line (Y = 0) for Equation 3.88 is $X_5 \pm r$, and the approximate limits of X in Equation 3.89 is $X_5 + r \pm r$. The hortest arrival time is for particles from the lowest point (center) of the cloud bottom, given by $(h - b)/v_5$, which is

$$t_f^o = 0.146W^{0.186} (1 - 0.0833W^{0.136}) \ hr; \ v_w \geq 3.28W^{0.246}$$ (3.90)

or

$$t_f^o = 0.186W^{0.254} (1 - 0.0833W^{0.136}) \ hr; \ v_w < 3.28W^{0.246}$$ (3.91)

The location on the pattern center line of earliest arrival is given by

$$X_c^o = v_w t_f^o$$ (3.92)

The earliest particle fall time at downwind locations outside the area of the limiting ellipses defined by Equations 3.88 and 3.89 is given by

$$t_f = X_c/v_w$$ (3.93)

41

where X_c is the downwind distance along the pattern center line to the center
of a constant arrival time ellipse. The distance to the center of the (half)
ellipse for an arbitrary point X, Y in the fallout area is defined by

$$X_c = X - r\sqrt{1 - Y^2/Y_o^2} \qquad \text{miles} \qquad (3.94)$$

In general, X_c must be solved by an iterative process using Equations 3.94 and
3.85. The number of iterations required to obtain a solution of X_c and Y_o to
within a few percent of the converged values is reduced if the first approxi-
mation of X_c in Equation 3.85 is taken to be equal to X - r if Y is less than
r, equal to X if Y is more than 2r, and equal to X - 0.5r if Y is between r
and 2r. If the iteration is done by computer, the last given first approxima-
tion of X_c could be used for all Y values.

The time for cessation (or last time of arrival) for all locations in
the cloud fallout pattern is estimated from Equations 3.83 and 3.93 with X_c
estimated from

$$X_c = X + r\sqrt{1 - Y^2/Y_o^2} \qquad \text{miles} \qquad (3.95)$$

together with Equation 3.85. If the center point of the constant arrival time
ellipse is selected, the value of Y_o from Equation 3.85 is obtained directly
and the arrival and cessation time contours are then calculated from Equations
3.94 and 3.95.

3.5.2 Dependence of Particle Fall Times and Other Parameters on Lateral Wind Shear

The particle fall times and scaling system parameters for the
larger particles that fall to the ground from stem heights are assumed to be
unaffected by lateral wind shear; thus lateral wind shear effects are considered
only for particles falling from cloud heights.

The methods described below for estimating the particle falling speeds and times and other parameters are for very simple lateral wind shear patterns. The basic assumptions for developing the mathematical representations are: (1) the lateral wind shear effect occurs only through the height range of the so-called stabilized cloud, i.e., from (h - b) to (h + b); (2) below the height, (h - b), all particles fall through the same set of meteorological conditions with a given average wind speed in the x direction, (thus the fall vectors of all particle groups for heights less than the bottom of the cloud, are parallel to the x axis); (3) the lateral wind shear through the height range of the cloud is either described by a given angle, θ_o, to the average direction of the wind below the cloud height or by a single valued parameter, designated as φ, in degrees per unit increase in height above the bottom of the cloud; (4) the magnitude of the fall vector for each group of particles remains constant from the height of origin in the cloud to the ground; and (5) the magnitude of the wind speed is constant at all altitudes (a minor assumption to simplify the mathematical representations).

The center of the cloud is taken as the center of the coordinate system; the periphery of the cloud is defined then by

$$b^2(x^2 + y^2) - r^2(b^2 - z^2) = 0 \qquad (3.96)$$

The time of fall of particles with a given value of v_f from a point x, y, z in the cloud to the bottom of the cloud is given by

$$t_b = (z + b)/v_f \qquad (3.97)$$

or

$$t_b = \frac{\left[(X_b - x)^2 + (Y_b - y)^2\right]^{1/2}}{v_w} \qquad (3.98)$$

where X_b, Y_b is the location of the particles in the z plane at (h - b) at the time, t_b. The lateral displacements are thus given by

43

$$X_b - x = (v_w/v_f)(z + b)\cos\theta \qquad (3.99)$$

and

$$Y_b - y = (v_w/v_f)(z + b)\sin\theta \qquad (3.100)$$

where

$$\theta = (z + b)\varphi \qquad \text{degrees} \qquad (3.101)$$

or, if θ is constant,

$$\theta = \theta_o \qquad \text{degrees} \qquad (3.102)$$

The time for the particle group to fall from the bottom of the cloud to the ground is given by

$$t_g = (h - b)/v_f \qquad (3.103)$$

or

$$t_g = (X - X_b)/v_w \qquad (3.104)$$

where X, Y, $(Y = Y_b)$ is the location at which the particles arrived on the ground and X is given by

$$X = X_b + (v_w/v_f)(h - b) \qquad (3.105)$$

or, in combination with Equation 3.99, by

$$X = x + (v_w/v_f)[(h - b) + (z + b)\cos\theta] \qquad (3.106)$$

The total time of fall is equal to $f_b + t_g$, given by

$$t_f = (z + h)/v_f \tag{3.107}$$

or

$$t_f = \frac{\left[(X - x)^2 + (Y - y)\right]^{1/2}}{v_w} \tag{3.108}$$

It should be noted that combinations of the above equations do not provide explicit solutions for cloud periphery values of x, y, and of z in terms of v_f and the cloud geometry equation constants when θ depends on z as given by Equation 3.101. A solution for v_f, however, is possible. (It may be noted that particles with the same value of v_f originating at different heights in the cloud do not have the same diameter; for particles with a given diameter, v_f is also a function of z.)

Estimates of the fall velocity of particles originating from the top and bottom of the cloud volume and landing at the point X, Y may be made from

$$v_f = v_w \frac{\left\{\left[(h - b)X + (z + b)(X\cos\theta + Y\sin\theta) \pm \sqrt{r^2(1 - z^2/b^2)\psi_1 - \psi_2^2}\right]\right\}}{X^2 + Y^2 - r^2(1 - z^2/b^2)} \tag{3.109}$$

where

$$\psi_1 = \left[(h - b) + (z + b)\cos\theta\right]^2 + (z + b)^2 \sin^2\theta \tag{3.110}$$

and

$$\psi_2 = (h - b)Y - (z + b)(X\sin\theta - Y\cos\theta) \tag{3.111}$$

for z values between -b and b. The limiting, or boundary, values among X, Y, and z at which real (as opposed to imaginary) values of v_f exist are obtained

45

by setting the quantities within the radical of Equation 3.109 equal to zero. The deposition pattern boundary lines for particle groups originating at the height $z + h$ at the periphery of the cloud ellipsoid are thus given by

$$Y_m = \frac{(z + b)X\sin\theta \pm r\sqrt{(1 - z^2/b^2)\psi_1}}{(h - b) + (z + b)\cos\theta} \qquad (3.112)$$

The corresponding values of the fall vector may be estimated from

$$v_f(m) = v_w\left\{\frac{[(h - b) + (z + b)\cos\theta] X + (z + b)Y_m\sin\theta}{X^2 + Y_m^2 - r^2(1 - z^2/b^2)}\right\} \qquad (3.113)$$

For a given value of X, Equation 3.112 represents a skewed elliptically-shaped curve in the Y_m, z coordinate system. The absolute maximum and minimum values of Y_m depend on both X and z. Although the slope of the lines in the X, Y plane increases as z increases from $-b$ to b, the value of the intercept at X equal to zero has a maximum for particles that fall from the center height of the cloud ($z = 0$). Thus, if no restriction on $v_f(m)$ is given and θ is positive, the largest variation $_m$ would be 2r at X equal to zero and would approach the value $2bX\sin\theta/[(h - b) + 2b\cos\theta]$ at very large values of X.

The general effect of lateral wind shear on the boundaries of the fallout patterns and on arrival and cessation times can be investigated through Equations 3.109 through 3.113. Although θ could have any value between zero and ±180 degrees, the average lateral wind shear at heights from 40,000 to 80,000 feet has been shown to be correlated with wind speed[12] whereby approximate values of φ can be estimated from

$$\varphi = 108\ v_w^{-1.14}\ \text{degrees/mile} \qquad (3.114)$$

for the summer season, and

$$\varphi = 38.3\ v_w^{-0.93}\ \text{degrees/mile} \qquad (3.115)$$

46

for the winter season; the applicable range of the two equations is for z + h values in the range of about 7 to 15 miles. Thus, for an integrated wind speed of 20 mi/hr, the average lateral shear angle from the bottom to the top of the cloud for a 1 MT yield explosion with a cloud thickness of 4.2 miles would be about 15° for the summer season and about 10° for the winter season. The data on which Equations 3.114 and 3.115 are based are limited and perhaps somewhat outdated; further studies of similar data would be desirable to determine the frequency of occurrence of larger lateral wind shear angles than the average angles obtained from the above equations.

If θ is assumed or taken to be independent of z, the following solutions of z, x, and y, are obtained (the solution for v_f is the same as that given by Equation 3.109 with θ replaced by θ_0).

$$z = \frac{v_w b^2 \left\{ \left(Y\sin\theta_0 + X\cos\theta_0 \right) v_f - v_w \left[b + (h - b)\cos\theta_0 \right] \right\}}{\left(r^2 v_f^2 + v_w^2 b^2 \right)}$$

$$\pm \frac{b \sqrt{\psi_3^2 - \left(v_f^2 r^2 + v_w^2 b^2 \right) \psi_4}}{\left(r^2 v_f^2 + v_w^2 b^2 \right)} \tag{3.116}$$

$$x = \frac{v_f^2 r^2 \left\{ X v_f - v_w \left[h - b \left(1 - \cos\theta_0 \right) \right] \right\} + v_w^2 b^2 \sin\theta_0 \left\{ \left[X v_f - v_w (h - b) \right] \sin\theta_0 - v_f Y\cos\theta_0 \right\}}{v_f \left(r^2 v_f^2 + v_w^2 b^2 \right)}$$

$$\pm \frac{v_w b\cos\theta_0 \sqrt{\psi_3^2 - \left(v_f^2 r^2 + v_w^2 b^2 \right) \psi_4}}{v_f \left(r^2 v_f^2 + v_w^2 b^2 \right)} \tag{3.117}$$

and

$$y = \frac{v_f^2 r^2 \left(Y v_f - v_w b\sin\theta \right) - v_w^2 b^2 \cos\theta_0 \left\{ \left[X v_f - v_w (h - b) \right] \sin\theta_0 - v_f Y\cos\theta_0 \right\}}{v_f \left(v_f^2 r^2 + v_w^2 b^2 \right)}$$

$$\pm \frac{v_w b\sin\theta \sqrt{\psi_3^2 - \left(r_f^2 v^2 + v_w^2 b^2 \right) \psi_4}}{v_f \left(v_f^2 r^2 + v_w^2 b^2 \right)} \tag{3.118}$$

where

$$\dot{v}_3 = r^2 v_f^2 + v_w b \left[(Y\sin\theta_o + X\cos\theta_o)v_f - v_w(h - b)\cos\theta_o \right] \qquad (3.119)$$

and

$$\dot{v}_4 = \left[v_f X - v_w(h - b) \right]^2 + v_f^2 Y^2 \qquad (3.120)$$

The limiting lateral extent of the fallout deposition, from the above equations, is defined by the condition that the Δz, or Δx and Δy segments within the cloud be equal to zero (which is the same as the limit for obtaining real values of x, y, and z; the limiting value of Y for a given value of v_f and X (with stated values of v_w and θ_o) is given by

$$Y_m = \frac{v_w b \sin\theta_o \left\{ r^2 v_f^2 + v_w b \cos\theta_o \left[X v_f - v_w(h - b) \right] \right\}}{v_f \left(r^2 v_f^2 + v_w^2 b^2 \cos^2\theta_o \right)}$$

$$\pm \frac{r \sqrt{\left(r^2 v_f^2 + v_w^2 b^2 \right) \left[r^2 v_f^2 + v_w^2 b^2 \cos^2\theta_o - \left\{ X v_f - v_w \left[h - b\left(1 - \cos\theta_o \right) \right] \right\}^2 \right]}}{\left(r^2 v_f^2 + v_w^2 b^2 \cos^2\theta_o \right)} \qquad (3.121)$$

An explicit equation for the limiting values of v_f for the fallout at a given location is not possible since the limiting equation contains terms of v_f with exponents from zero to 4. The values of v_f that give maximum and minimum values of Y_m at any value of X may be estimated from

$$v_f^o(\text{max}) = (v_w/X) \left\{ (h - b) + \left[\frac{r^2(h - b)b + b\cos\theta_o)^2}{2r^2(h - b)b^2\cos\theta_o + (X + b\cos\theta_o)^2} \right] 2b\cos\theta_o \right\} \qquad (3.122)$$

48

and

$$v_f^o(\text{min}) = (v_w/X)\left\{(h - b) + \frac{2r^2(h - b)b^2\cos\theta_o}{r^2(h - b)b + \left[X + 2(h - b)\cos\theta_o\right]^2}\right\} \tag{3.123}$$

Substitution of Equations 3.122 and 3.123 into Equation 3.121 gives the following general equation for the boundaries of the fallout as a function of the downwind distance, X,

$$Y_m^o = \frac{bX\sin\theta_o\left\{r^2\psi_m^2 + \left[\psi_m - (h - b)\right]bX\cos\theta_o\right\}}{\psi_m\left(r^2\psi_m^2 + b^2X^2\cos^2\theta_o\right)}$$

$$\pm \frac{r\sqrt{\left(r^2\psi_m^2 + b^2X^2\right)\left[r^2\psi_m^2 + b^2X^2\cos\theta_o - X^2\left\{\psi_m - \left[h - b\left(1 - \cos\theta_o\right)\right]\right\}^2\right]}}{\left(r^2\psi_m^2 + b^2X^2\cos\theta_o\right)} \tag{3.124}$$

in which

$$\psi_m = \psi_{\text{max}} = Xv_f^o(\text{max})/v_w \tag{3.125}$$

and

$$\psi_m = \psi_{\text{min}} = Xv_f^o(\text{min})/v_w \tag{3.126}$$

as obtained from Equations 3.122 and 3.123 respectively. The notations (min) and (max) refer to the v_f values giving the smallest and largest values of Y_m rather than the smallest and largest values of v_f.

The effect of lateral shear within the height range of the cloud thickness is illustrated by the following values of Y_m^o calculated for a 1 MT yield cloud and θ_o value of 30° (note that v_w does not appear in Equation 3.124):

49

X (miles)	Y^{o}_{max} (miles)	Y^{o}_{min} (miles)	ΔY^{o}_{m} (miles)	$\Delta Y^{o}_{m}/2r$
10	10.3	-8.1	18.4	1.01
20	11.5	-7.2	18.7	1.03
50	15.5	-4.9	20.4	1.12
100	23.2	-3.0	26.2	1.44
500	94.0	-0.1	94.1	5.17

The overall pattern spread at 100 miles away from ground zero for 30° of shear results in only a 44 percent increase in the apparent pattern width relative to the "stabilized" cloud diameter. Although the center line of the pattern is slightly curved, the angle between the center line and the X axis to a distance of 50 or 100 miles for the illustration, is about 6°.

3.5.3 Dependence of Particle Fall Times and Their Parameters on Total Wind Shear

For overall wind shear effects, variation in wind speed as well as direction over the range of cloud thickness must be taken into account. To illustrate, the very simple shear condition is assumed in which v_{w} is the integrated wind speed up to the height of the cloud bottom and in which the integrated wind speed increases at a constant rate of S miles/hr per mile at greater heights (a variation in speed with height may also occur at lower heights, which would be accounted for in the integrated speed to the cloud bottom; this integrated wind speed would be approximately the same for all v_{f} if time variations in the wind speeds and directions at all z are not considered). The angle between the direction of the integrated wind speed vector to the bottom of the cloud and the direction of the wind above the bottom of the cloud is designated as θ. The direction of the integrated wind speed vector to the bottom of the cloud is defined to be parallel to the X axis. With these definitions and assumptions, the wind speed over the height range of the cloud is represented by

$$v_{w}(z) = v_{w} + (z + b)S \qquad (3.127)$$

50

With Equation 3.127, an explicit solution for x, y, and z cannot be obtained for the given cloud geometry; however, the values of v_f for particle groups originating at the height $z + h$ on the cloud periphery and landing at the point X, Y may be estimated from

$$v_f = \frac{v_w(h - b)X + \left[v_w + (z + b)S\right](z + b)(X\cos\theta + Y\cos\theta)}{X^2 + Y^2 - r^2(1 - z^2/b^2)}$$

$$\pm \frac{\sqrt{r^2(1 - z^2/b^2)\psi_5 - \psi_6^2}}{X^2 + Y^2 - r^2(1 - z^2/b^2)} \tag{3.128}$$

where

$$\psi_5 = \left\{v_w(h - b) + \left[v_w + (z + b)S\right](z + b)\cos\theta\right\}^2$$

$$+ \left[v_w + (z + b)S\right]^2(z + b)^2\sin^2\theta \tag{3.129}$$

and

$$\psi_6 = v_w(h - b)Y - \left[v_w + (z + b)S\right](z + b)(X\sin\theta - Y\cos\theta) \tag{3.130}$$

The maximum values of Y for the particles originating at the height $(z + h)$ and landing at the downwind distance X are given by

$$Y_m = \frac{\left[v_w + (z + b)S\right](z + b)X\sin\theta \pm r\sqrt{(1 - z^2/b^2)}\psi_5}{v_w(h - b) + \left[v_w + (z + b)S\right](z + b)\cos\theta} \tag{3.131}$$

Although an explicit equation for the maximum and minimum values of Y_m is not readily obtained, approximate values can be derived graphically. The effect of total shear on the spread of the pattern is illustrated by the following

51

values of Y_m^O calculated for a 1 MT yield cloud, a θ_o value of 30°, a v_w of 15 mi/hr, and an S value of 2.1 per hour:

X	Y_{max}^O	Y_{min}^O	ΔY_m^O	$\Delta Y_m^O/2r$
(miles)	(miles)	(miles)	(miles)	
10	10.6	-7.9	18.5	1.02
20	12.3	-6.8	19.1	1.05
50	17.8	-4.6	22.4	1.23
100	28.4	-2.8	31.2	1.71
500	124.7	-0.1	124.8	6.85

The overall pattern spread at 100 miles away from ground zero for 30° of lateral shear and an S value of 2.1 per hour of height above the bottom of the cloud results in a 171 percent increase in the apparent pattern width relative to the "stabilized" cloud diameter. The average angle between the center line of the pattern and the X axis at a downwind distance of 100 miles is slightly larger than 7°. The values of v_f for the particle group that land at X, Y_m are given by the first term of Equation 3.128.

The lateral displacement of particles with a given value of v_f originating at the height z + h on the cloud periphery and landing at the downwind distance X may be illustrated from

$$Y = \frac{\left[v_w + (z + b)S \right] (z + b)\sin\theta}{v_f} \pm$$

$$\frac{\sqrt{v_f^2 r^2 \left(1 - z^2/b^2 \right) - \left\{ \left[v_w + (z + b)S \right] (z + b)\cos\theta - \left[Xv_f - v_w(h - b) \right] \right\}^2}}{v_f} \quad (3.132)$$

The limiting value of v_f for all real values of Y in terms of z and X are given by

$$v_f(X) = \frac{v_w(h - b) + \left[v_w + (z + b)S\right](z + b)\cos\theta}{X \pm r\sqrt{1 - z^2/b^2}} \tag{3.133}$$

and the corresponding lateral displacement limits from Equation 3.132, are

$$Y(X) = \frac{\left[v_w + (z + b)S\right](z + b)\sin\theta \left[X \pm r\sqrt{1 - z^2/b^2}\right]}{v_w(h - b) + \left[v_w + (z + b)S\right](z + b)\cos\theta} \tag{3.134}$$

The equations for $v_f(X)$ and $Y(X)$ give the envelopes of these two variables at a given value of X for all particle groups within the cloud volume. The paired values of each are for the particles originating from the cloud ellipse at y equal to zero. The general shapes of the v_f envelopes are shown in Figure 3.4 for X equal to 50 and 100 miles. In addition, specific variations of v_f with z + b are shown for the X, Y points of 50,10 and 100,15. For each of these curves, the values of z + b and v_f that give the minimum and maximum of v_f and t_f are indicated; the points of tangency with the envelopes are also shown as well as the major parameter values used in the calculations.

An explicit general solution for z in terms of other parameters is not possible; the general equation of z is

$$b^2 S^2 z^4 + 2bS(v_w b + 2S)z^3$$

$$+ \left\{ \left[v_f^2 r^2 - 2b^2 S(X\cos\theta + Y\sin\theta) \right] + v_w b^2 \left[v_w + 2S(\ldots\ldots)\cos\theta \right] + 6b^2 S(v_w + bS) \right\} z^2$$

$$+ 2b^2 (v_w + 2bS)\left[b(v_w + bS) + v_w(h - b)\cos\theta - v_f(X\cos\theta + Y\sin\theta) \right]z$$

$$+ b^3(v_w + bS)\left\{ b(v_w + bS) - 2\left[v_f(X\cos\theta + Y\sin\theta) - v_w(h - b)\cos\theta \right] \right\}$$

$$+ b^2\left[Xv_f - v_w(h - b) \right]^2 + v_f^2(Y^2 - r^2) = 0 \tag{3.135}$$

Approximate representations of the fallout pattern boundaries and the general directions of the boundaries, range of v_f values, and times of arrival

53
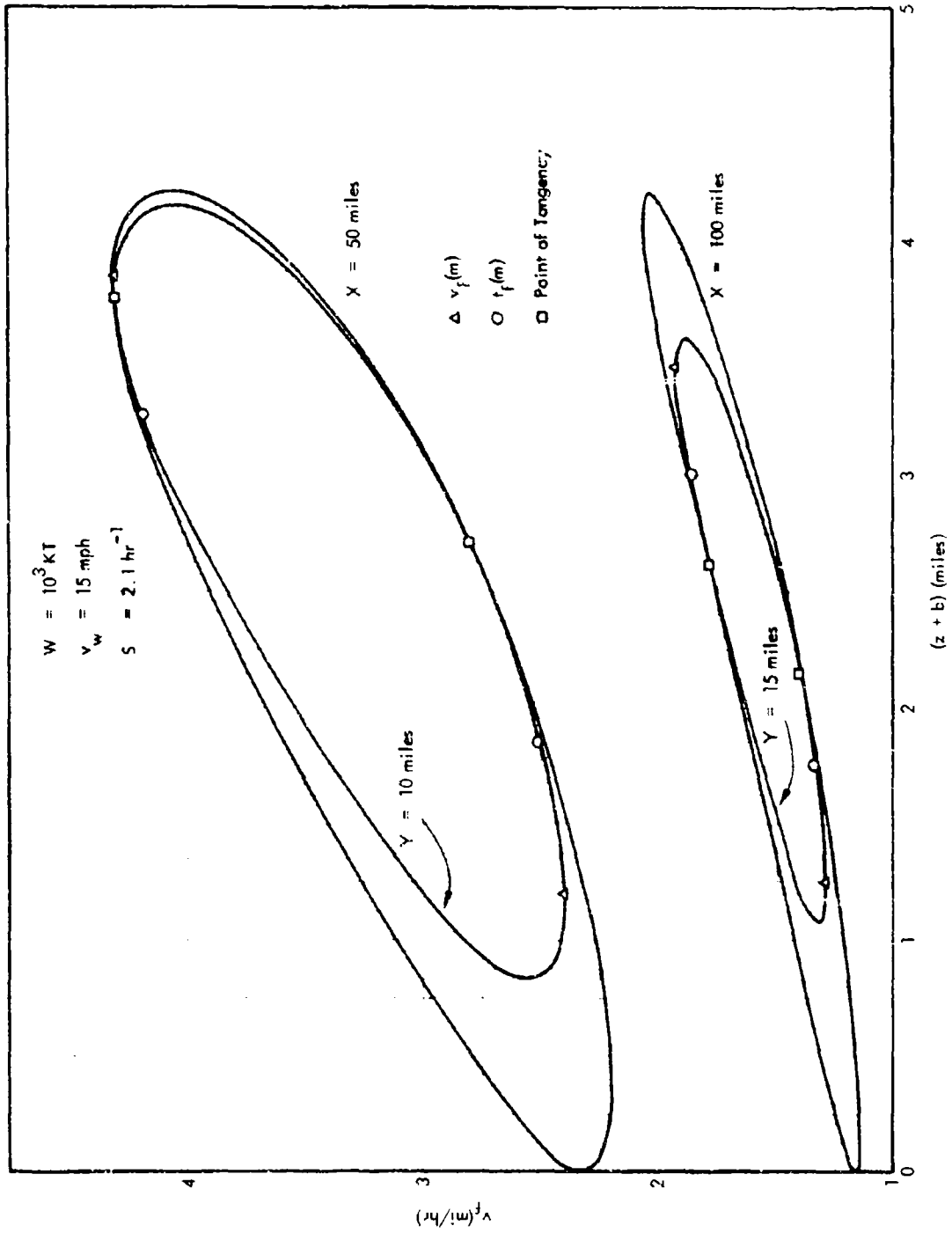
Fig. 3.4.   Variation of v_f with $z + b$ Showing Envelopes at X Equal to 50 and 100 Miles and Specific Variations for X, Y Locations 50, 10 and 100, 15

and cessation at locations may be given in relation to the particle tra-
jectories from the center of the cloud originating at a given height along
with the dimensions of the circular disc enclosing the area covered by the
particles. The latter is given by

$$(X - X_c)^2 + (Y - Y_c)^2 = r^2(1 - z^2/b^2) \tag{3.136}$$

where

$$X_c = \frac{v_w(h - b) + \left[v_w + (z + b)S\right](z + b)\cos\theta}{v_f} \tag{3.137}$$

and

$$Y_c = \frac{\left[v_w + (z + b)S\right](z + b)\sin\theta}{v_f} \tag{3.138}$$

The paired values of X_c and Y_c, or the line on the X, Y plane along which the
particles with any value (originating at the height $z + b$ at the center of the
cloud) are deposited, is given by

$$Y_c = \frac{\left[v_w + (z + b)S\right](z + b)X_c\sin\theta}{v_w(h - b) + \left[v_w + (z + b)S\right](z + b)\cos\theta} \tag{3.139}$$

The values of z for particles with a given range in v_f values landing at
the location X_c, Y_c, from rearrangement of Equation 3.139 may be estimated from

$$z = \frac{1}{2S} \sqrt{v_w^2 + \frac{4v_w S(h - b)Y_c}{\left(X_c\sin\theta_o - Y_c\cos\theta_o\right)}} - (v_w + 2bS) \tag{3.140}$$

In Equations 3.137 to 3.139, the angle θ may be a function of z; however, the
separation of the two variables in Equation 3.140 indicates the assumption
that θ is independent of z. The value of v_f for the particle disc centered
at X_c, Y_c, and origination at the height $z + h$ in the cloud is represented by

$$v_f = \frac{v_w(h - b)\sin\theta_o}{X_c\sin\theta_o - Y_c\cos\theta_o} \qquad (3.141)$$

The value of Y_m, from combination of the above equations with Equation 3.138, in terms of X_c and Y_c is given by

$$Y_m = Y_c \pm (r/X_c)\sqrt{X_c^2 + Y_c^2} \qquad (3.142)$$

The time of fall from the height $z + h$ of the particle disc centered at X_c, Y_c, may be estimated from Equation 3.107 or from

$$t_f = \frac{\left(X_c\sin\theta_o - Y_c\sin\theta_o\right)}{2v_w S(h - b)\sin\theta_o} \quad 2S(h - b) + \sqrt{v_w^2 + \frac{4v_w(h - b)Y_c}{\left(X_c\sin\theta_o - Y_c\cos\theta_o\right)}} \qquad (3.143)$$

It may be noted that while Equation 3.136 defines the area covered by a circular disc in the X, Y plane centered at the location X_c, Y_c, it defines a skewed elliptically shaped curve in the X_c, Y_c plane having a pseudo-center at the location X, Y; such a curve represents the loci of the particle disc centers on the X_c, Y_c plane for those discs whose radius is just equal to the distance between the disc center and the location X, Y. Thus the particles with the largest and smallest values of v_f and t_f that deposit at the location X, Y are those on the edge of four different particle discs that originate at four different heights and whose centers are at four different X_c, Y_c locations. The values of X_c for particles landing at X, Y originating at the height $z + h$ (and located at the edge of the particle disc) is given by

$$X_c = \frac{\left\{v_w(h - b) + \left[v_w + (z + b)S\right](z + b)\cos\theta\right\}}{\psi_5} \times$$

$$\frac{\left\{v_w(h - b)X + \left[v_w + (z + b)S\right](z + b)(X\cos\theta + Y\sin\theta)\right\}}{\psi_5}$$

$$\pm \frac{\left\{v_w(h - b) + \left[v_w + (z + b)S\right](z + b)\cos\theta\right\}\sqrt{r^2(1 - z^2/b^2)\psi_5 - \psi_6^2}}{\psi_5} \qquad (3.144)$$

56

The corresponding values of Y_c may be calculated from Equation 3.139. The variation of Y_c with X_c for the cited conditions for the X, Y locations 50,10 and 100,15 is shown in Figure 3.5. The X_c, Y_c locations of the particle discs that are first and last to arrive (designated t_a and t_c, respectively), that originate at the cloud mid-height (z = 0), and that originate from the maximum and minimum heights in the cloud (Z_{max} and Z_{min}, respectively) are indicated on each of the two curves. The X_c, Y_c locations of the discs giving the maximum and minimum values of v_f and t_f are obtained graphically from a plot of t_f as a function of v_f. The respective values of these parameters are as follows:

X_c (miles)	Y_c (miles)	v_f (mi/hr)	t_f (hr)	(z + b) (miles)
X = 50, Y = 10				
50.39	2.74	2.552	3.37	0.836
55.99	4.37	2.406	3.73	1.200
58.51	6.96	2.508	3.83	1.850
42.53	8.50	4.191	2.63	3.262
44.91	10.32	4.309	2.70	3.850
49.49	12.09	4.081	2.92	4.154

X = 100, Y = 15				
100.56	7.07	1.319	6.71	1.080
104.98	8.39	1.288	6.98	1.225
108.55	12.25	1.334	7.13	1.750
92.04	17.13	1.868	5.77	3.003
95.23	20.06	1.926	5.83	3.468
98.62	21.36	1.890	6.00	3.584

No explicit equations have been derived for estimating the maximum and minimum values of v_f, t_f, and z for the particles deposited at an arbitrarily selected X, Y location.

57
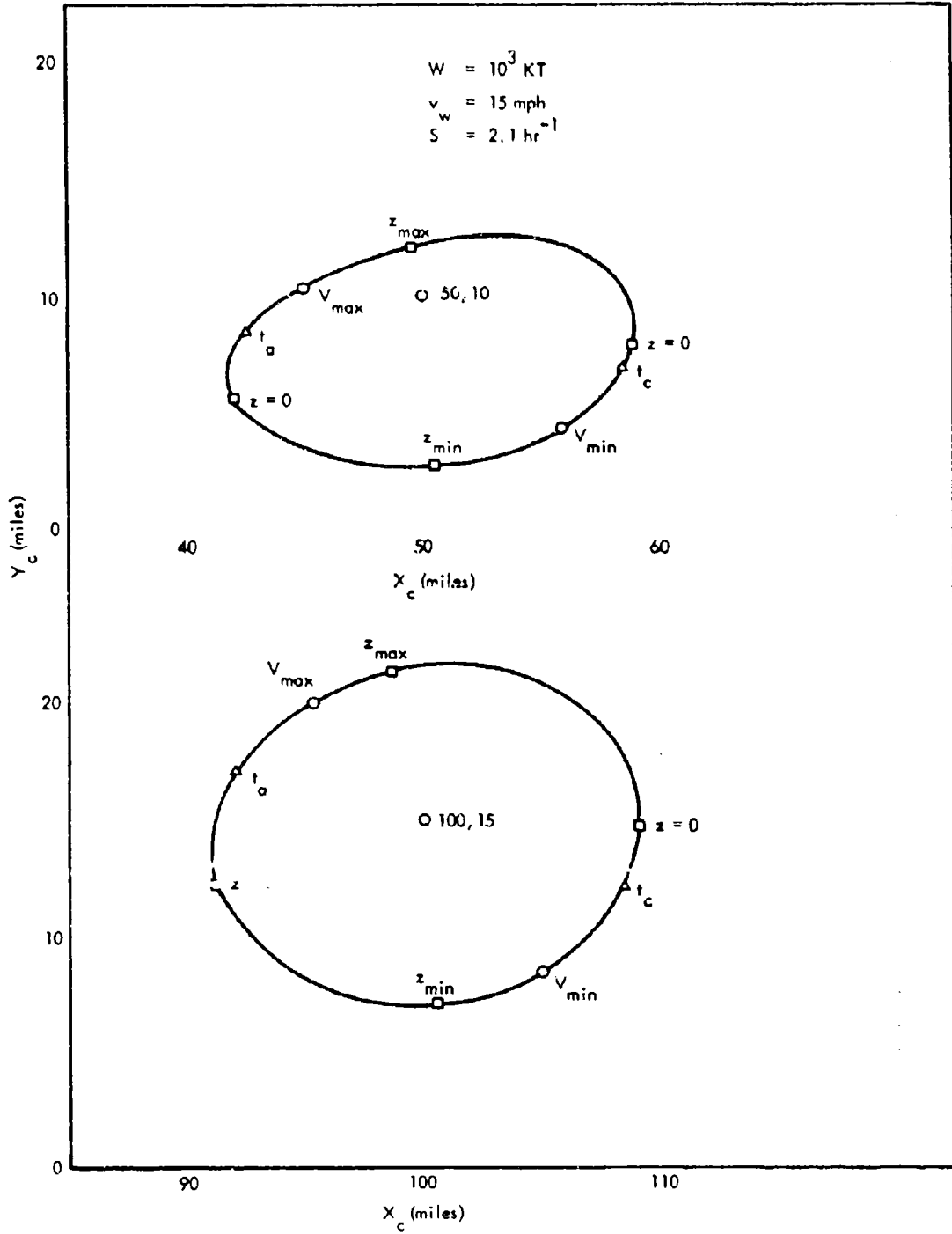
Fig. 3.5. Variation of Y_c with X_c for X, Y Locations 50, 10 and 100, 15

3.5.4 Wind Speed and Shear Definitions for the Fallout Pattern Scaling Systems

As previously discussed,[4] the fallout pattern scaling system coefficients were, to a large degree, evaluated from data on the fallout distributions from test shots Jangle S and Castle Bravo. Relative wind data for these two detonations are applied here to illustrate some definitions of wind speed and shear that are applicable to the scaling system.

In general, the integrated wind speed refers to the total displacement of an imaginary particle of undefined size falling with constant speed from a given height (or altitude) to another height or to the ground. Thus, an integrated wind speed may be directly obtained from balloon sounding data. Where the latter are given as a function of azimuth and speed for given altitude increments, then $\bar{v}_w^o(Z)$, the integrated wind speed from the ground surface to the height, Z, is calculated from

$$\bar{v}_w^o(Z) = \frac{\displaystyle\sum_{i=1}^{i=n} v_i \Delta Z_i \sin\theta_i}{Z \sin\theta_n^o} \qquad (3.145)$$

where ΔZ_i is the thickness of the ith altitude increment, v_i is the wind speed of the itn altitude increment, Z is the height or altitude of the nth increment, and θ_n^o is obtained from

$$\tan\theta_n^o = \frac{\displaystyle\sum_{i=1}^{i=n} v_i \sin\theta_i}{\displaystyle\sum_{i=1}^{i=n} v_i \cos\theta_i} \qquad (3.146)$$

The average (unidirectional) wind speed is, in similar units, defined by

$$\bar{v}_w^o = \frac{\displaystyle\sum_{i=1}^{i=n} v_i \Delta Z_i}{Z} \qquad (3.147)$$

The integrated (or average) particle displacement speeds for particles falling from large heights are usually less than the integrated wind speeds since solid particles (and especially those with large diameters) fall faster at the higher altitudes than at the lower altitudes. The integrated particle displacement speeds are given by

$$v_w(Z) = \frac{\displaystyle\sum_{i=1}^{i=n} v_i \Delta t_i \sin\theta_i}{t_n \sin\theta_n} \qquad (3.148)$$

where Δt_i is the time of fall through the ith altitude increment, t_n is the total time of fall through the n altitude increments, and θ_n is obtained from

$$\tan\theta_n = \frac{\displaystyle\sum_{i=1}^{i=n} v_i \Delta t_i \sin\theta_i}{\displaystyle\sum_{i=1}^{i=n} v_i \Delta t_i \cos\theta_i} \qquad (3.149)$$

both Δt_i and t_n, for a given altitude increment and total distance of fall, vary with particle diameter.

If the wind speeds and directions remain constant over the period of fall of all the particles of interest from all Z, then a single value of $\bar{v}_w(Z)$ and $\bar{v}_w^o$ for each Z is obtained. This condition may be approximately met for clouds from small yield detonations and for t_n values of less than 2 to 3 hours. But for clouds from large yield detonations where t_n is greater than 2 to 3 hours even for fairly large particles, it is much less likely that the wind speeds and directions will remain constant in time at even one location; they generally are also not likely to be constant over the deposition area because of the resulting larger displacement distances.

60

The results from displacement calculations (details to be given in a following report) for the Jangle S Shot and Castle Bravo Shot clouds are summarized in Tables 3.6 and 3.7, respectively.

The computed values of $\bar{v}_w^0(Z)$, $v_w(Z)$ for particle diameters from 75 to 400 microns and $\bar{v}_w^0$ are all about the same for the Jangle S Shot cloud; also, the $\bar{\theta}_n$ values differ very little from θ_n^0 for the integrated wind speed. However, because of the higher altitudes, variation of the wind speeds and azimuths with time (and space), and large changes in angle with altitude, the values of $\bar{v}_w^0(Z)$, $v_w(Z)$, and $\bar{v}_w^0$ for the Castle Bravo Shot show much larger differences; the same is true for $\bar{\theta}_n$ and θ_n^0. The maximum difference in $\bar{\theta}_n$ is 8.5 for the particles from the Jangle S cloud and 2$\subset$ ° for the 1 0-micron particles from the Castle Bravo cloud.

The accumulated (or integrated) shear factors relative to the height of the bottom of the cloud and the angular displacements for particles of different diameters are summarized in Tables 3.8 and 3.9 for the Jangle S and Castle Bravo Shot clouds, respectively. The total shear factor for the Jangle S Shot cloud is quite large, mainly due to the increase in wind speed with height above the cloud bottom; in addition, the values of both $\bar{S}$ and $\bar{\theta}$ are about the same for all the particle diameters from 75 to 400 microns. The values of S and $\bar{\theta}$ for the particles with 100- and 200-micron diameters from the Castle Bravo cloud include time and space variation; the variation in $\bar{\theta}$ with height is the major source of shear since the displacement of the particles starting at the top of the cloud is almost $180°$ from the directions of the hodograph of particles falling from the bottom of the cloud to the ground.

The above described angular and total shear effects are included in the fallout pattern scaling functions. This fact should be kept in mind in applying the functions; in no case are the scaling functions directly applicable to a no-wind shear condition (i.e., the patterns always will contain residual effects of this shear, irrespective of the values of $\bar{v}_w$ used in the calculations). If a single wind speed and direction is assumed for all altitudes (a condition

Table 3.6

SUMMARY OF INTEGRATED WIND AND PARTICLE DISPLACEMENT
SPEEDS AND DIRECTIONS FOR THE JANGLE S SHOT CLOUD

Wind or Particle Displacement	$Z - h_b$, (10^3 ft)					
	0	0.11	1.11	1.48	2.11	2.96
	$\bar{v}_w^o(Z)$ or $\bar{v}_w(Z)$, (mi/hr)					
Average Wind Speed	25.1	25.4	27.8	28.7	30.0	31.5
Integrated Wind Speed	24.8	25.1	27.4	28.3	29.5	30.9
Particle Displacement Speed						
d = 75 microns	24.6	24.9	27.2	28.0	29.3	30.6
d = 100 microns	24.6	24.9	27.2	28.0	29.2	30.6
d = 200 microns	24.6	24.9	27.2	28.0	29.2	30.6
d = 400 microns	24.5	24.8	27.1	27.9	29.1	30.5
	θ_n^o or θ_n (degrees)					
Integrated Wind	184.8	185.1	188.5	189.6	191.2	193.3
Particle Displacement						
d = 75 microns	184.7	185.0	188.3	189.4	191.1	193.1
d = 100 microns	184.7	185.0	188.2	189.4	191.0	193.1
d = 200 microns	184.6	185.0	188.2	189.4	191.0	193.0
d = 400 microns	184.6	184.9	188.2	189.3	190.9	193.0

Table 3.7

SUMMARY OF (RELATIVE) INTEGRATED WIND AND PARTICLE DISPLACEMENT
SPEEDS AND DIRECTIONS FOR THE CASTLE BRAVO SHOT CLOUD

Wind or Particle Displacement

	$Z - h_b$, $(10^3\ ft)$
	0	3.75	13.75	23.75	25.06	33.75	43.75	50.12
	$v_w^c(Z)$ or $\bar{v}_w(Z)$
Average Wind Speed (d = 100 μ)	28.9	28.5	27.0	27.5	27.7	28.9	33.5	35.8
Average Wind Speed (d = 200 μ)	26.7	26.2	24.7	25.4	25.6	27.0	31.7	34.2
Integrated Wind Speed (d = 100 μ)	22.1	21.2	19.3	13.6	13.0	8.5	0.6?	3.9
Integrated Wind Speed (d = 200 μ)	21.3	20.1	18.0	12.3	11.6	7.1	3.3	6.1
Particle Displacement Speed								
d = 100 microns	19.6	19.1	18.0	14.4	14.0	11.0	6.3	3.8
d = 200 microns	18.2	17.6	16.4	13.1	12.7	10.0	6.2	3.9
	θ_n^o or θ_n
Integrated Wind (d = 100 μ)	250.6	254.0	261.1	262.5	264.2	271.7	4.9	47.1
Integrated Wind (d = 200 μ)	251.0	254.6	263.8	267.7	270.3	280.7	279.1	69.1
Particle Displacement								
d = 100 microns	254.8	257.6	264.5	267.0	268.2	273.2	268.6	278.7
d = 200 microns	253.0	255.6	260.7	261.4	262.3	265.0	255.0	254.8

63

Table 3.8

ACCUMULATED SHEAR FACTORS AND ANGLES FOR THE
JANGLE S SHOT CLOUD

Particle Diameter		$Z - h_b$, $(10^3$ ft$)$			
(microns)	0	1.11	1.48	2.11	2.96
		$v_w(Z)$, (mi/hr)			
75	$(24.6)^a$	41.8	42.5	43.3	43.7
100	(24.6)	41.7	42.6	43.3	43.8
200	(24.6)	41.9	42.7	43.4	43.8
400	(24.5)	40.8	42.5	43.2	43.7
		θ, (degrees)			
75	$(184.7)^a$	15.0	15.9	16.6	18.0
100	(184.7)	14.9	15.8	16.6	18.0
200	(184.6)	14.8	15.8	16.6	18.0
400	(184.6)	14.7	15.7	16.7	18.0
		S, $(hr)^{-1}$			
75	-	81.4	63.8	46.6	34.1
100	-	81.5	64.1	46.7	34.1
200	-	82.3	64.4	46.9	34.2
400	-	8?.5	64.6	46.7	34.2

a Values in parenthesis are for the integrated particle displacements
from h_b.

64

Table 3.9

ACCUMULATED SHEAR FACTORS AND ANGLES FOR THE
CASTLE BRAVO CLOUD

$z - h_b$ (10^3 ft)	$v_w(z)$ (mi/hr) 100 μ	$v_w(z)$ (mi/hr) 200 μ	θ (degrees) 100 μ	θ (degrees) 200 μ	s (hr^{-1}) 100 μ	s (hr^{-1}) 200 μ
0	$(19.6)^a$	$(18.2)^a$	$(254.8)^a$	$(253.0)^a$		
3.75	23.7	17.9	70.2	30.1	5.73	-0.46
8.75	21.9	16.3	64.7	69.6	1.35	-1.16
13.75	22.4	16.9	72.6	78.0	1.07	-0.51
18.75	17.9	13.1	86.8	96.6	-0.48	-1.44
23.75	15.7	12.8	114.3	131.0	-0.88	-1.22
25.06	16.4	13.6	116.9	132.9	-0.68	-0.98
28.75	18.3	15.8	124.3	138.2	-0.25	-0.44
33.75	19.4	17.6	138.1	151.7	-0.031	-0.10
38.75	22.3	20.9	148.5	159.4	0.37	0.36
43.75	24.0	23.3	168.6	178.0	0.53	0.62
48.75	27.9	27.0	169.5	177.8	0.89	0.95
50.12	29.2	28.0	170.8	179.0	1.00	1.03

a   Values in parenthesis are for the integrated particle displacements
from h_b

that corresponds to the average unidirectional wind speed defined above), then the computed average wind speed must be reduced by a factor of 15/28.7 (or 0.52) when using the scaling functions for yields less than 30 KT and by a factor of 15/26.6 (or 0.56) when using the scaling functions for yields larger than 30 KT.[*] These corrections are only approximate ones for the larger weapon yields; the correction factor actually should vary with particle size. However, these corrections will give a first order approximation of the pattern scaling function values when a single average wind speed is used. Revisions and extensions of the fallout pattern scaling system that are now in progress should minimize the wind speed correction problem; the major question to be resolved is whether the adjustments can be properly introduced without also introducing additional and more involved computational steps into the system.

3.5.5 Distribution of the Condensed Radioactivity Among Particles as a Function of Falling Velocity Vector of Particle Diameter

The activity carried by particles with a given value of v_f falling from stem altitudes is conveniently represented by

$$i_f'(1) = K_f(1)A_f' \qquad R/hr \text{ at } 1 \text{ hr} \qquad (3.150)$$

where A_f' is the activity in fissions/ft^2 for a unit area of the stem (of specified thickness) at the altitude from which the particles assume gravity fall, and $K_f(1)$ is the conversion factor from fissions/ft^2 to R/hr at 1 hr for the particle group. The total activity deposited at a given downwind distance in the stem fallout pattern is calculated from

$$I_s = 1.467v_w \int_{v_f(min)}^{v_f(max)} (K_f(1)A_f'/v_f^2)dv_f \qquad R/hr \text{ at } 1 \text{ hr} \qquad (3.151)$$

---

[*] No correction to the wind speed for the stem fallout pattern is suggested; for most applications a wind speed of 15 mi/hr should be used.

where $v_f(min)$ and $v_f(max)$ are the limiting fall velocity vectors in ft/sec for the smallest and largest particles that are deposited (as described in Section 3.5.1), and v_w is the average wind speed in mi/hr from the surface to Z_f. In the described scaling system for the stem fallout, only those particles with a given value of v_f arrive at a given time; the arrival time for each particle group is given by the sum of Equations 3.73 and 3.74 (or 3.75 and 3.76); thus the activity deposited up to a given time after detonation is calculated by graphical integration represented by

$$I_s(t) = 3.38 v_w \int_{v_f(t)}^{v_f(max)} (K_f(1)A_f'/v_f^2) dv_f \qquad R/hr \text{ at } 1 \text{ hr} \qquad (3.152)$$

where $v_f(t)$ is the fall vector of the particle group arriving at t [$v_f(max)$ being the fall vector of the first particles that arrive]. The ionization rate at a given time is calculated by multiplying $I_s(t)$ by a decay correction factor, $\bar{d}_f(t)$ so that

$$I(t) = \bar{d}_f(t)I_s(t) \qquad (3.153)$$

where $\bar{d}_f(t)$ is the average ratio of the ionization rate at the time, t, to the rate at H + 1 for all the particles that are deposited at the location. If a large variation in the gross decay with particle sizes is to be assumed, then $d_f(t)$ could be applied in Equation 3.152 prior to the indicated integrations.

To estimate the above integrals and the fallout deposition rates, the variation of $i_f'(1)$ with v_f must first be computed from the stem fallout pattern scaling functions. This is done by using the variation of I_s with X, for $X \geq (X_2 + X_3)/2$ and $v_w = 15$ mph, along the center line of the stem fallout pattern and, in the first approximation, taking a single value of $K_f(1)A_f'$ in Equation 3.151 for the particles that fall at a location. The single (average) value of $K_f(1)A_f'$ is then written as

67

$$K_f(1)A_f' = \frac{I_s}{1.467v_w\left[1/v_f(min) - 1/v_f(max)\right]} \quad \text{R/hr at 1 hr} \quad (3.154)$$

The first estimate of the value of v_f, for association with each $K_f(1)A_f'$ value is computed from

$$\log \bar{v}_f = -0.050 + 0.769W^{0.048}\log v_f(min); \quad W \simeq 10^3 \text{ to } 5 \times 10^4 \text{ KT} \quad (3.155)$$

or

$$\log \bar{v}_f = 0.070 + 1.25W^{-0.043}\log v_f(max); \quad W \simeq 10^3 \text{ to } 5 \times 10^4 \text{ KT} \quad (3.156)$$

or from the average of the $\bar{v}_f$ values computed from both equations. The adjusted values of $K_f(1)A_f'/v_f^2$ as a function of v_f are determined from successive approximations of I_s in Equation 3.151 starting with $\overline{K_f(1)A_f'}$ for $K_f(1)A_f'$ and $\bar{v}_f$ for v_f.

The activity deposited by particle groups with a given fall vector from cloud altitudes at a given downwind location, for the simple fallout pattern scaling system in which a uniform distribution of each particle throughout the cloud volume is assumed, is represented by

$$i_f(1) = \frac{2K_f(1)A_f br^{-1}\sqrt{\left(v_f^2 + v_w^2b^2r^{-2}\right)r^2 - \left(v_f - v_whX^{-1}\right)^2X^2}}{\left(v_f^2 + v_w^2b^2r^{-2}\right)} \quad \text{R/hr at 1 hr}$$

$$(3.157)$$

for locations on the fallout center line with either a directionally balanced effective (or no) lateral wind shear. In Equation 3.157, A_f is the average initial cloud concentration in fissions/ft^3 of the activity carried by the particles with the fall vector v_f, $K_f(1)$ is the conversion factor in R/hr at 1 hr per fission/ft^2, and the remaining combined terms represent the path length through the elliptical cloud from which the particles with the fall vector v_f originate and which deposit at the downwind distance X on the pattern center line. Integration of $i_f(1)$ over all the particle groups that land at the location gives the total activity deposited; this is represented by

68

$$I_s = 1.467 v_w \int_{v_f(min)}^{v_f(max)} (i_f(1)/v_f^2) dv_f \qquad \text{R/hr at 1 hr} \qquad (3.158)$$

for v_w in mi/hr and v_f in ft/sec.

The average deposition rate of the particle group with the fall vector, v_f, from the cloud altitudes is given by

$$i_f(1)/\Delta t_f = 3.6 \times 10^3 v_f K_f(1) A_f \qquad \text{R/hr at 1 hr/hr} \qquad (3.159)$$

where Δt_f is the time period over which particles with a given value of v_f land on the ground; Δt_f may be obtained from a plot of t_f as a function of v_f; for locations near the pattern center line, for the case of no wind shear, it is given by

$$\Delta t_f = \frac{2b \sqrt{\left(v_f^2 + v_w^2 b^2 r^{-2}\right) - \left(v_f - v_w h X^{-1}\right) X^2 r^{-2}}}{\left(v_f^2 + v_w^2 b^2 r^{-2}\right)} \qquad (3.160)$$

The deposition rate of all the particle groups arriving at a given time after detonation at a location is represented by

$$(dI_s/dt)_t = 5.28 \times 10^3 v_w \int_{v_f(min,t)}^{v_f(max,t)} (K_f(1) A_f/v_f) dv_f \qquad \text{R/hr at 1 hr/hr} \qquad (3.161)$$

Integration of Equation 3.161 gives, for $I_s(t)$,

$$I_s(t) = 5.28 \times 10^3 v_w \int_{t_a}^{t} dt \int_{v_f(min,t)}^{v_f(max,t)} \frac{K_f(1)A_f}{v_f} dv_f \quad \text{R/hr at 1 hr} \tag{3.162}$$

The estimates of $K_f(1)A_f$ for difference values of v_f are made through a series of approximations starting with selected values of I_s and the downwind distance along the center line of the cloud fallout pattern at which they are calculated to occur, using the simplified scaling system with a 15 mph average wind speed. The following equations may be utilized to provide the first estimates of $K_f(1)A_f$ and v_f (designated at $\overline{K_f(1)A_f}$ and $\overline{v_f}$, respectively) for each set of paired values of I_s and X.

$$\overline{K_f(1)A_f} = \frac{I_s}{1.128 \times 10^4 w^{0.431} \log \varphi_f(X)} \tag{3.163}$$

where

$$\varphi_f(X) = \frac{(X + r) + \sqrt{r^2 h^2 b^{-2} + (X + r)^2}}{(X - r) + \sqrt{r^2 h^2 b^{-2} + (X - r)^2}}, \quad X > r \tag{3.164}$$

and

$$\varphi_f(X) = \frac{(X + r) + \sqrt{r^2 h^2 b^{-2} + (X + r)^2}}{X_o + \sqrt{r^2 h^2 b^{-2} + X_o^2}}, \quad X \le r \tag{3.165}$$

in which

$$r = 0.464W^{0.431} \text{ miles}, \quad W = 1 \text{ to } 10^5 \text{ KT}$$

$$r^2 h^2 b^{-2} = 31.00W^{0.590} \text{ sq. mi.}, \quad W = 30 \text{ to } 10^5 \text{ KT}$$

$$X_0 = 0.186v_w W^{0.254} \text{ miles}, \quad W = 30 \text{ to } 10^5 \text{ KT}$$

The first estimate of v_f for each value of $\overline{K_f(1)A_f}$ is obtained from

$$\overline{v_f} = \frac{70.0W^{0.164}}{X} \text{ ft/sec}; \quad X > r; \quad W = 30 \text{ to } 10^5 \text{ KT} \qquad (3.166)$$

for X in miles. If the estimates are made using wind speed other than 15 mi/hr, the coefficient 70.0 is replaced with $4.67v_w$ (for v_w in mi/hr).

The potential exposure dose during the fallout arrival period is calculated by integrating graphically the computed values of $I(t)$ from t_a to t_c for the fallout from both stem and cloud altitudes. Also, the value of $K_f(1)$ is adjusted to eliminate the instrument response factor, t, of equation 3.65; this correction, for the $I_s(t)$ values computed through use of the simplified fallout scaling system, requires increasing the integrated doses by a factor of 1.33.

Because the rather complicated form of the above equations giving the variation of $I_s(t)$ and $I(t)$ with time after detonation, only a few example calculations were made from which approximating functions were derived to represent the variation of $I_s(t)$ or the accumulation of the fallout from stem and cloud heights with time after detonation. Since the model of the stem depicts the fall of the larger particles from lower heights in combination with the gradual dilution of the particle concentrations with height (and time) and the deduced activity-size distribution (from the arrangement of the stem fallout pattern), a fallout rate given as $dI_s(t)/dt$ is obtained that is highest at the first arrival of fallout and decreases as an inverse function of time during the fallout period. On the other hand, the model for the

fallout from the cloud wherein the particles are assumed to fall from a
stationary source volume of uniform concentration, the fallout rate increases
from zero at the first arrival of fallout, increases to a maximum, and then
decreases to zero again at fallout cessation. This general picture of the
deposition rates is fairly well verified by analysis of observed intensity
(exposure rate) data; however, detailed data from time-interval collectors
show large short-time variabilities in the deposition rates which indicates
that the particles are not uniformly distributed in the source volumes.
(Some of the observed variability in the collector data is undoubtedly also
caused by local variations in the surface wind speeds and directions over the
deposition period and the apparent efficiency of the collectors.)

The simplified versions of the increase of $I_s(t)$ with time during the
fallout period are given in terms of the fraction of I_s that is deposited at
a given fraction of the deposit period; the representation is defined by

$$I_s(t) = f(t)I_s \qquad (3.167)$$

and the fraction of the time during the deposition period is defined by

$$\tau = (t - t_a)/(t_c - t_a) \qquad (3.168)$$

For the fallout from stem heights with $f(t)$ redesignated as f_s, the above-
described variation of the fallout rates with time is represented approximately
by

$$df_s/d\tau = \frac{f_s^o \sqrt{1 - (2\tau - 1)^2}}{\tau} \qquad (3.169)$$

where f_s^o is a constant; integration of Equation 3.169 under the condition that
f_s is zero when τ is zero and f_s is equal to one at τ equal to one gives

$$f_s = (1/\pi)\left[\sqrt{1 - (2\tau - 1)^2} + \sin^{-1}(2\tau - 1)\right] + 0.500 \qquad (3.170)$$

where f_s^o is equal to $1/\pi$.

72

For the fallout from cloud heights with $f(t)$ redesignated as f_c, the above-described variation of the fallout rates with time is represented approximately by

$$df_c/dt = f_c^0 \sqrt{1 - (2\tau - 1)^2} \qquad (3.171)$$

for a symmetrical rate of arrival curve that has a peak rate of arrival at the mid-time of fallout period (i.e., at $\tau = 0.5$). Integration of Equation 3.171 gives

$$f_c = (1/\pi)\left[(2\tau - 1)\sqrt{1 - (2\tau - 1)^2} + \sin^{-1}(2\tau - 1)\right] + 0.500 \qquad (3.172)$$

In regions of heavier fallout from the cloud heights, the peak fallout rate generally occurs somewhat earlier in the fallout period than at the mid-time, more nearly at the time of τ equal to 0.4 than 0.5. The equations for f_c with the peak rate of fallout at τ equal to 0.4 are

$$f_c = (1/\pi)\left[(2.5\tau - 1)\sqrt{1 - (2.5\tau - 1)^2} + \sin^{-1}(2.5\tau - 1)\right]$$
$$+ 0.500; \ \tau \leq 0.4 \qquad (3.173)$$

and

$$f_c = (1/\pi)\left[(1.67\tau - 0.67)\sqrt{1 - (1.67\tau - 0.67)^2} + \sin^{-1}(1.67\tau - 0.67)\right]$$
$$+ 0.500; \ \tau \geq 0.4 \qquad (3.174)$$

The calculated variation of f_s and of f_c with τ is given in Figures 3.6 and 3.7, respectively. The curves can be used directly for estimating $I(t)$; for the cloud fallout, and the values of f_c taken from the curves for τ_0 equal 0.4 would be preferred. At the shorter downwind distances the peak fallout rate may occur even earlier in the fallout period; also, the time of the peak

73
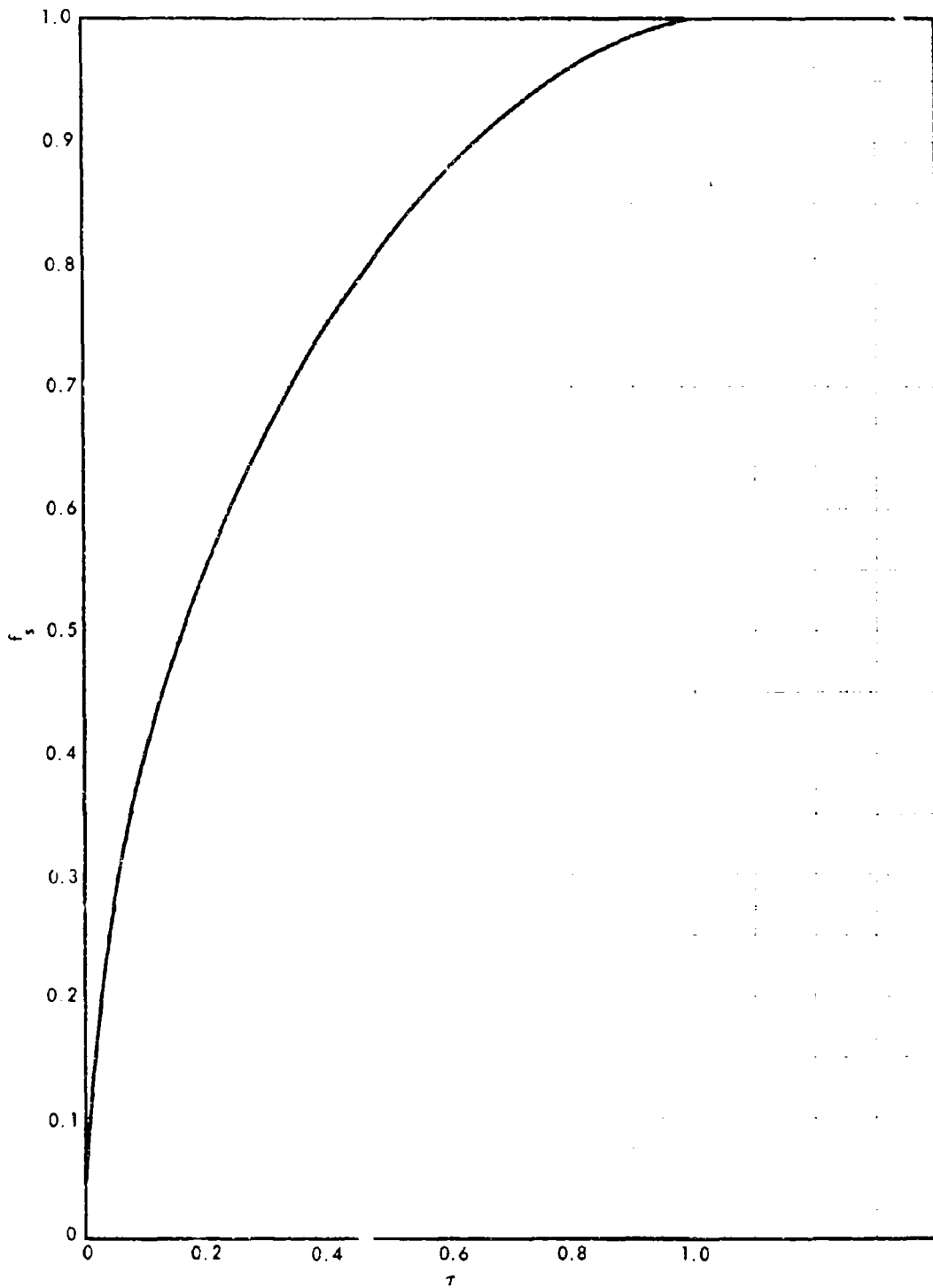
Fig. 3.6.   Variation of f_s with τ for Stem Fallout
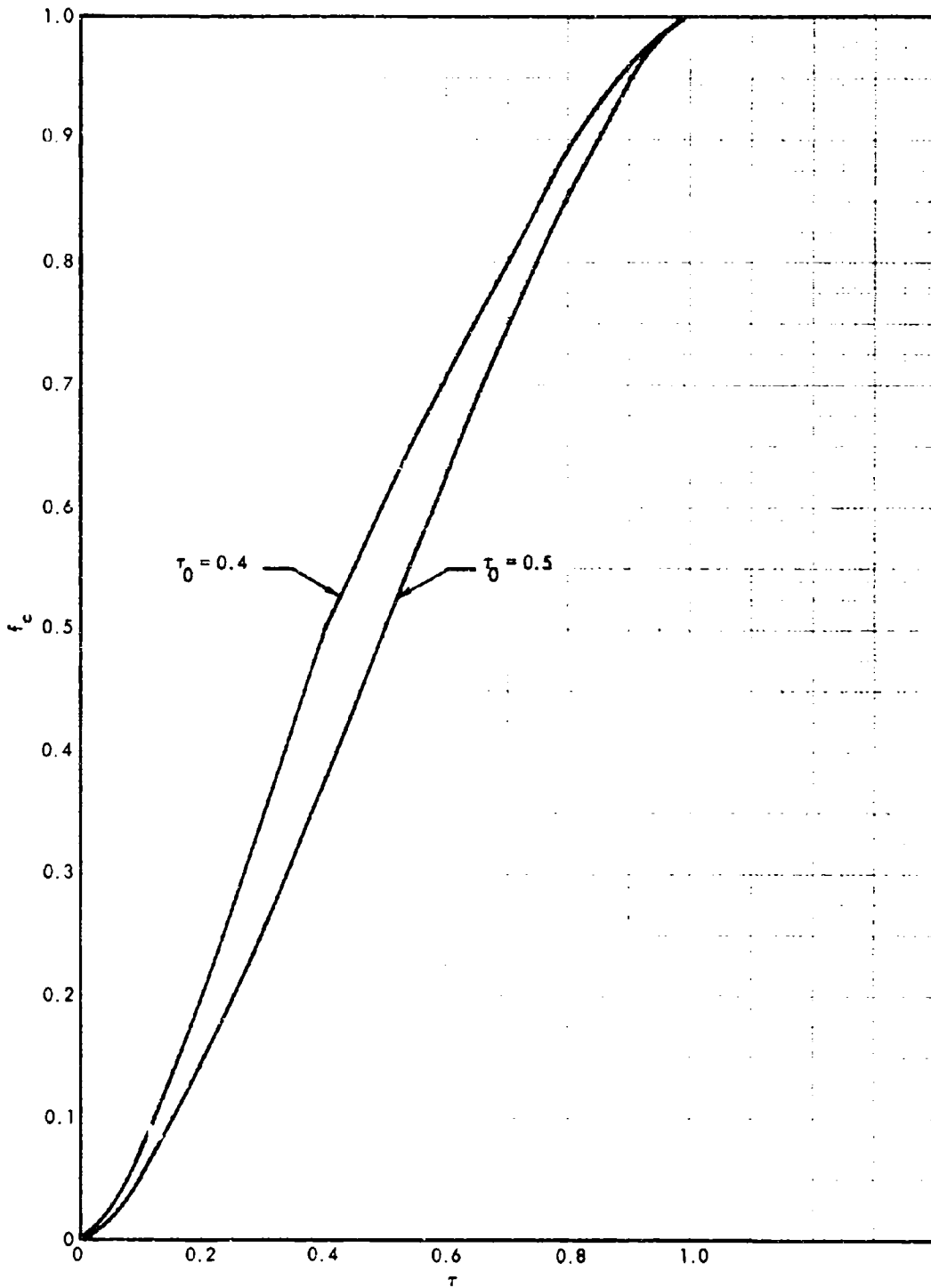
Fig. 3.7.   Variation of f_c with τ for Cloud Fallout

ra'e would tend to shift towards the mid-time as the downwind distance becomes very large. The approximations for f_s and f_c given by Equations 3.170, 3.173, and 3.174 are consistent with the model formulation for application to computer programming in damage assessment evaluations.

To illustrate the shapes of the $I(t)$ curves as a function of time after detonation, values of this variable were calculated for the following assumed conditions; for the stem fallout, t_a is 0.5 hrs, t_c is 1.0 hr, I_s is 1,000 R/hr at 1 hr, and $d(t)$ is equal to $1/t$; for the cloud fallout, t_a is 1.0 hr, t_c is 2.0 hr, I_s is 1,000 R/hr at 1 hr, and $d(t)$ is equal to $1/t$. Since, in general,

$$t = t_a + (t_c - t_a)\tau \qquad (3.175)$$

then

$$t = 0.5 + 0.5\tau \qquad (3.176)$$

for the assumed stem fallout case, and

$$t = 1 + \tau \qquad (3.177)$$

for the assumed cloud fallout case. Also,

$$I(t) = 1,000 \, f_s/t \qquad (3.178)$$

for the stem fallout, and

$$I(t) = 1,000 \, f_c/t \qquad (3.179)$$

for the cloud fallout. The calculated values of $I(t)$ for the two assumed sets of conditions are plotted as a function of t in Figure 3.8. The peak intensity
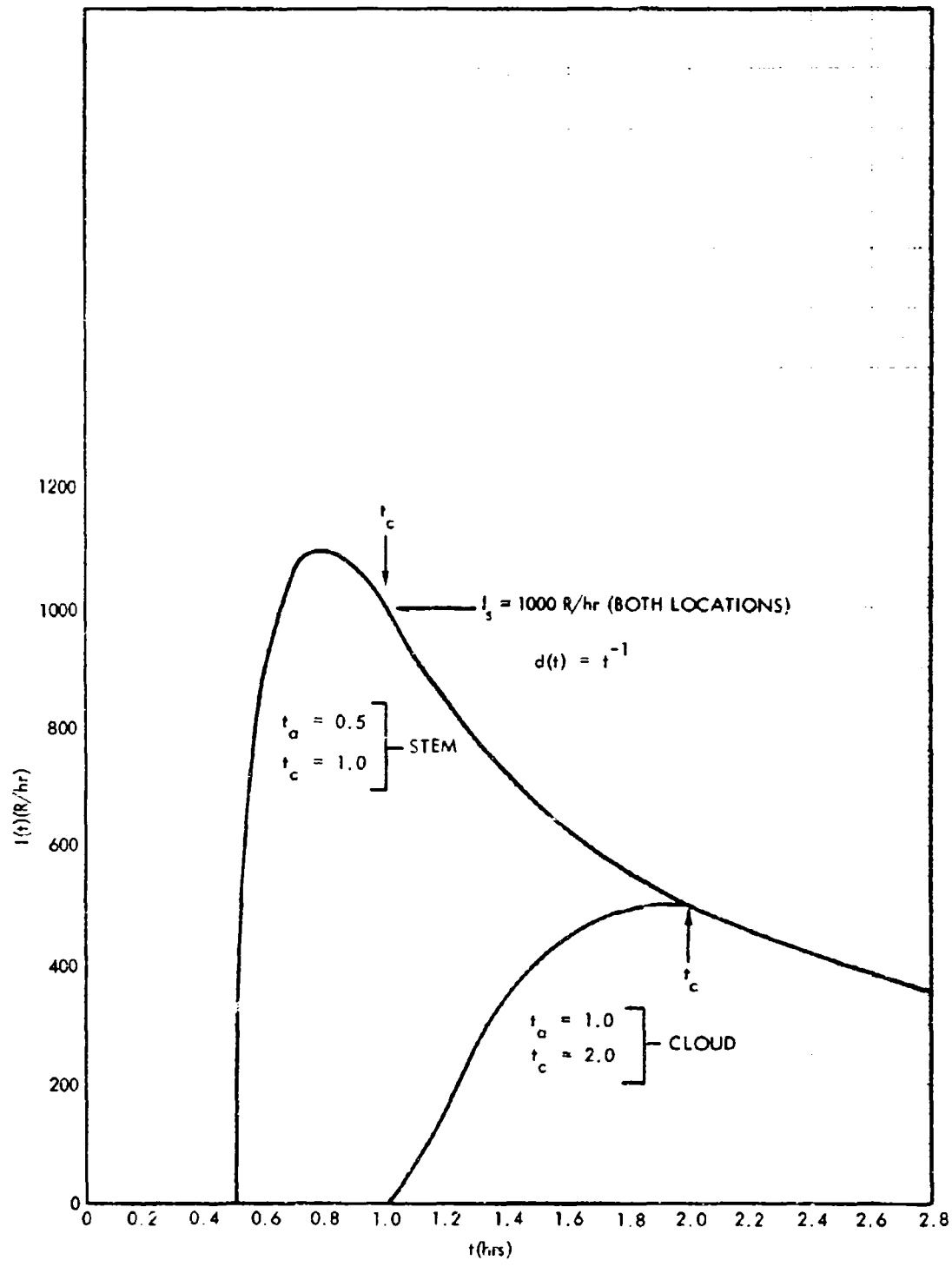
Fig. 3.8. Variation of I(t) with Time After Detonation for Two Assumed Sets of Conditions

77

for the assumed stem fallout case is almost 1,100 R/hr and it occurs at about 0.8 hrs ($\tau = 0.6$). The peak intensity for the assumed cloud fallout case is 505 R/hr and it occurs at about 1.9 hrs ($\tau = 0.9$).

The air ionization rate from the airborne particles can be estimated from either the calculated deposition rates or the estimates of $K_f(1)A_f$. From calculations made by Laumetz,[16] the air ionization rate at three feet inside a plane boundary of a semi-infinite volume containing a uniformly-distributed radiation source is given by

$$I_a(t) = 0.950 \times 10^{-6} A_t A_o(t) E_t \text{ in R/hr} \tag{3.180}$$

in which A_t is the activity in dis/sec per fission at the time, t, after fission, $A_o(t)$ is the concentration in fissions/ft^3, and E_t is the total gamma ray energy in Mev/dis.

At a given time, A_t and E_t are constant, so that the contributions to activity in A_f from all the particle groups arriving at a given time can be summed as in the case of the deposited material. Multiplication by the appropriate values of A_t and E_t for the designated time will convert the sum to R/hr. The fallout from stem altitudes arriving at a given instant consists of particles with a single value of v_f whose air activity concentration is estimated from

$$A_o(t) = \frac{1}{K_f(1)v_f(t)} \left(\frac{dI(t)}{dt}\right) \text{ fissions/ft}^3 \tag{3.181}$$

The values of A_o for the fallout from cloud altitudes arriving at a given instant is estimated from

$$A_o(t) = 3.38 v_w \int_{v_f(\min,t)}^{v_f(\max,t)} (A_f/v_f)(d \log v_f) \text{ fissions/ft}^3 \tag{3.182}$$

78

in which A_f is equal to $i_f/K_f(1)$ for the particles arriving at the time, t, and where v_w is in mi/hr and v_f is in ft/sec.

SUMMARY

This report summarizes the fallout pattern scaling relationships that were developed in the period 1962 to 1964; the report includes the values of the scaling equation coefficients that were derived from selected fallout pattern data. The meaning of the scalar wind speed multiplier that is used in the scaling equations is discussed relative to computer applications of the scaling system and approximate wind speed adjustment factors for use with wind speed averages that may be assumed in such applications are provided. The relative degree of wind shear inherent in the scaling system parameters is also discussed in some detail. Basic equations for relating surface density of radionuclides and air ionization rates including consideration of fractionation, surface roughness, and instrument response are given and discussed together with the influence of these factors and others on the limiting values of K factors that represent the relative amount of the radioactive sources contained within the deduced area covered by the fallout patterns. Scaling equations and data are also presented for use in estimating, for any location in the fallout region, the time of fallout arrival, the time of fallout cessation, the variation of the exposure rate (i.e., air ionization rate in roentgens per hour) with time during fallout arrival, and the total potential exposure from the time of fallout arrival to selected later times.

REFERENCES

1. Kellogg, W. W., Hearings before the Special Subcommittee on Readiation of the Joint Committee on Atomic Energy, U.S. Congress, The Nature of Radioactive Fallout and Its Effects on Man, Part I, p. 104 – 41, 1957

2. Anderson, A. D., A Theory for Close-In Fallout, USNRDL-TR-249, U.S. Naval Radiological Defense Laboratory, 1958.

3. Kellogg, W. W., R. R. Rapp, and S. M. Greenfield, J. Meteor. 14, 1, 1 – 8, 1957

4. Miller, C. F., Fallout and Radiological Countermeasures, SRI Project 4021, Stanford Research Institute, January 1963

5. Schuert, E. A., A Fallout Forecasting Technique with Results Obtained at the Eniwetok Proving Ground, USNRDL-TR-139, U.S. Naval Radiological Defense Laboratory, 1957

6. Miller, C. F., "Formation of Fallout Particles," Chapter 2, Biological and Radiological Effects of Fallout from Nuclear Explosions, SRI Project 4536, Stanford Research Institute, March 1964

7. Ksanda, D. V., L. Minvielle, and A. Moskin, Scaling of Contamination Patterns, Surface and Underground Detonations, USNRDL-TR-1, U.S. Naval Radiological Defense Laboratory, 1953 (Classified)

8. Laurino, R. K., and I. G. Poppoff, Contamination Patters at Operation JANGLE, USNRDL-399, U.S. Naval Radiological Defense Laboratory, 1953 (Classified)

9. Capabilities of Atomic Weapons, Armed Forces Special Weapons Project, TM-23-200, 1958 (Classified)

10. The Effects of Nuclear Weapons, U.S. Government Printing Office, Washington, D. C. 1957, revised 1962

11. Anderson, A. D., <u>Application of "Theory for Close-In Fallout" to Low-Yield Land Surface and Underground Nuclear Detonations</u>, USNRDL-TR-289, U.S. Naval Radiological Defense Laboratory, 1959

12. Pugh, G. E., and R. J. Galiano, <u>An Analytic Model of Close-In Deposition of Fallout for Use in Operational-Type Studies</u>, Research Memorandum No. 10, Weapons Systems Evaluations Group, 1959

13. Callahan, E. D., L. Rosenblum, J. D. Kaplan, and D. R. Batten, <u>The Probable Fallout Threat Over the Continental United States</u>, TO-B60-13 1960

14. Rapp, R. R., Summary Report of RAND Work on the AFSWP Fallout Project, RM-2334, 1959 (Classified)

15. Cassidy, S. H., Private Communication, U.S. Naval Radiological Defense Laboratory, 1963

16. Laumetz, E., Private Communication, U.S. Naval Radiological Defense Laboratory, 1960

Appendix A

SUMMARY OF SELECTED SCALING SYSTEM PARAMETERS

Provisional values of several of the fallout scaling system model parameters for weapon yields in the range of 1 to 30 KT, not provided in the main text of the report, are as follows:

$$X_2 \simeq 0.0139W^{0.494} \left[v_w - 10.34W^{-0.167} \right] \text{ miles; } W = 1 \text{ to } 30 \text{ KT} \tag{A-1}$$

$$X_3 \simeq 0.0139W^{0.494} \left[v_w + 10.34W^{-0.157} \right] \text{ miles; } W = 1 \text{ to } 30 \text{ KT} \tag{A-2}$$

$$X_4 \simeq 0.0973v_w W^{0.550} \text{ miles; } W = 1 \text{ to } 30 \text{ KT} \tag{A-3}$$

$$Z_{2,3} = 3.43 \times 10^3 W^{0.414} \text{ feet; } W = 1 \text{ to } 30 \text{ KT} \tag{A-4}$$

$$I_{2,3} = 3.483 \times 10^4 v_w^{-m_w} W^{1.122}; \ W = 1 \text{ to } 30 \text{ KT} \tag{A-5}$$

$$m_w = 0.793; \ W = 1 \text{ to } 30 \text{ KT} \tag{A-6}$$

$$X_1 = -0.385W^{0.496} \text{ miles; } (v_w = 15 \text{ mi/hr}); \ W = 1 \text{ to } 30 \text{ KT} \tag{A-7}$$

$$X_1 = X_2 - 0.139W^{0.404} \log I_{2,3}; \ W = 1 \text{ to } 30 \text{ KT} \tag{A-8}$$

$$X_5 = 0.0556v_w W^{0.467} \text{ miles; } W = 1 \text{ to } 30 \text{ KT} \tag{A-9}$$

$$X_6 = 0.0894v_w W^{0.481} \text{ miles; } W = 1 \text{ to } 30 \text{ KT} \tag{A-10}$$

$$X_7 = 0.0919v_w W^{0.586} \text{ miles; } W = 1 \text{ to } 30 \text{ KT} \tag{A-11}$$

$$X_8 = 0.128v_w W^{0.596} \text{ miles; } W = 1 \text{ to } 30 \text{ KT} \tag{A-12}$$

$$X_9 = 1.956v_w W^{0.319} \text{ miles; } W = 1 \text{ to } 30 \text{ KT} \tag{A-13}$$

$$v_5 r/h = 8.34W^{-0.03} \text{ mi/hr; } W = 1 \text{ to } 30 \text{ KT} \tag{A-14}$$

$$v_6 r/h = 5.19W^{-0.050} \text{ mi/hr; } W = 1 \text{ to } 30 \text{ KT} \tag{A-15}$$

$$v_7 r/h = 5.04W^{-0.155} \text{ mi/hr; } W = 1 \text{ to } 30 \text{ KT} \tag{A-16}$$

The values of K_1^o, m_1, $(v_1^2 r^2 b^{-2})_1^o$, and r_1 for the yield range of 1 to 30 KT are the same as those given in Table 3.1 for application in Equations 3.28 and 3.30.

Calculations of fallout arrival times for average wind speeds of 10, 20, and 30 mi/hr at selected downwind (X) and crosswind (Y) distances for weapon yields of 1, 3, and 10 MT are summarized in Tables 1A, 2A, and 3A, respectively. The wind speed corrections discussed in paragraph 3.5.4 do not apply to the arrival time calculations. Similar calculations on the fallout cessation times are summarized in Tables 4A, 5A, and 6A.

Calculations of the exposure dose during the fallout period and from fallout cessation to H + 36 at selected X,Y locations are summarized in Table 7A in terms of Exposure Dose-Standard Intensity Ratios for a detonation yield of 1 MT and an average wind speed of 20 mi/hr. The calculations show that $D(36)/I_s$ is essentially independent of Y at a given value of X. The values of $D(36)/I_s$ are represented very closely by

$$D(36)/I_s = 3.16 \, e^{-9.79 \times 10^{-3} X}; \quad X \leq 85 \text{ km, All Y} \tag{A-17}$$

and

$$D(36)/I_s = 1.73 \, e^{-2.72 \times 10^{-3} X}; \quad X \geq 85 \text{ km, All Y} \tag{A-18}$$

for W = 1,000 KT, v_w = 20 mi/hr, and X in km. The additive exposure doses for times greater than H + 36 may be obtained from the so-called dose-rate multipliers (DRM) given in Volume II of Reference 4. The variation of $I(t)/I_s$ with time after detonation for downwind distances of 10, 20, 50, 150, 250, and 350 km is illustrated in Figures 1-A through 6-A.

Table 1A

SUMMARY OF TIME OF ARRIVAL OF FALLOUT FROM CLOUD HEIGHTS
AT SELECTED X,Y LOCATIONS FOR W = 1,000 KT
(Time in Hours After Detonation)

± Y (km)

X (km)	0	5	10	20	40	60	80	100	120	140
				1. $v_w = 10$ mi/hr						
10	0.94	0.94	0.94	0.96	1.12					
20	0.95	0.95	0.96	0.97	1.07					
30	1.04	1.04	1.06	1.12	1.36					
50	2.28	2.84	2.29	2.32	2.44	2.65				
150	8.50	8.50	8.50	8.51	8.55	8.61	8.71	8.87	9.14	
250	14.71	14.71	14.71	14.72	14.75	14.80	14.88	15.00	15.18	
350	20.93	20.93	20.93	20.94	20.96	21.01	21.09	21.19	21.36	21.71
				2. $v_w = 20$ mi/hr						
10	0.49	0.49	0.51							
20	0.50	0.50	0.52							
30	0.56	0.58	0.68	0.81						
50	1.18	1.19	1.21	1.30						
150	4.29	4.29	4.30	4.32	4.40	4.60				
250	7.40	7.40	7.40	7.41	7.46	7.57				
350	10.51	10.51	10.51	10.52	10.56	10.64	10.81			
450	13.61	13.61	13.62	13.63	13.66	13.74	13.88			
550	16.72	16.72	16.72	16.73	16.77	16.84	16.97			
650	19.83	19.83	19.83	19.84	19.88	19.94	20.08			
750	22.94	22.94	22.93	22.95	22.98	23.05	23.18			
				3. $\bar{v}_w = 30$ mi/hr						
10	-	-	-	-	-	-				
20	0.49	0.50	0.52							
30	0.51	0.52	0.55							
50	0.82	0.83	0.87							
150	2.89	2.89	2.90	2.93	3.09					
250	4.96	4.96	4.97	4.98	5.06					
350	7.02	7.03	7.04	7.05	7.10	7.24				
450	9.10	9.10	9.11	9.12	9.16	9.26				
550	11.18	11.18	11.18	11.19	11.23	11.32				
650	13.25	13.25	13.25	13.26	13.30	13.38				
750	15.32	15.32	15.32	15.33	15.37	15.45				
850	17.39	17.39	17.39	17.40	17.44	17.52				
950	19.46	19.46	19.46	19.47	19.51	19.59				
1050	21.53	21.54	21.54	21.54	21.58	21.66				
1150	23.61	23.61	23.61	23.62	23.65	23.73				

Table 2A

SUMMARY OF TIME OF ARRIVAL OF FALLOUT FROM CLOUD HEIGHTS
AT SELECTED X,Y LOCATIONS FOR W = 5,000 KT

Y (km)

X (km)	0	5	10	20	40	60	80	100	120	140

1. v_w = 10 mi/hr

X (km)	0	5	10	20	40	60	80	100	120	140
10	1.16	1.17	1.17	1.19	1.27					
20	1.15	1.15	1.15	1.17	1.23					
30	1.20	1.20	1.20	1.21	1.28					
50	1.72	1.73	1.74	1.78	1.95	2.23				
150	7.94	7.94	7.94	7.95	7.99	8.07	8.18	8.33	8.54	8.86
250	14.15	14.15	14.15	14.16	14.19	14.24	14.31	14.41	14.55	14.73
350	20.37	20.37	20.37	20.38	20.40	20.44	20.51	20.59	20.71	20.86

2. v_w = 20 mi/hr

X (km)	0	5	10	20	40	60	80	100	120	140
10	-	-	-							
20	1.29	1.31	-							
30	1.15	1.16	1.17	1.22						
50	1.21	1.21	1.22	1.26						
150	4.01	4.01	4.01	4.04	4.14	4.36				
250	7.11	7.12	7.12	7.13	7.19	7.30	7.48			
350	10.22	10.22	10.23	10.24	10.28	10.36	10.48	10.72		
450	13.33	13.33	13.33	13.34	13.38	13.44	13.55	13.72		
550	16.44	16.44	16.44	16.45	16.48	16.54	16.63	16.79		
650	19.54	19.55	19.55	19.55	19.59	19.64	19.73	19.87		
750	22.65	22.65	22.65	22.66	22.69	22.75	22.83	22.97	23.27	

3. v_w = 30 mi/hr

X (km)	0	5	10	20	40	60	80	100	120	140
10	0.58	0.59	0.65							
20	0.55	0.57	0.58							
30	0.56	0.56	0.58							
50	0.65	0.66	0.71							
150	2.70	2.70	2.71	2.75	2.95					
250	4.77	4.77	4.77	4.79	4.88	5.09				
350	6.84	6.84	6.84	6.86	6.92	7.04				
450	8.91	8.91	8.92	8.93	8.97	9.06	9.26			
550	10.98	10.98	10.99	11.00	11.04	11.11	11.25			
650	13.06	13.06	13.06	13.07	13.10	13.17	13.29			
750	15.13	15.13	15.13	15.14	15.17	15.23	15.35			
850	17.20	17.20	17.20	17.21	17.24	17.30	17.40			
950	19.27	19.27	19.27	19.28	19.31	19.37	19.47			
1050	21.34	21.34	21.34	21.35	21.38	21.44	21.54	21.79		
1150	23.41	23.41	23.42	23.42	23.45	23.51	23.60	23.84		

A.4

Table 3A

SUMMARY OF TIME OF ARRIVAL OF FALLOUT FROM CLOUD HEIGHTS
AT SELECTED X,Y LOCATIONS FOR W = 10,000 KT

Y (km)

X (km)	0	5	10	20	40	60	80	100	120	140

1. v_w = 10 mi/hr

X (km)	0	5	10	20	40	60	80	100	120	140
10	1.46	1.46	1.48	1.48	1.54	1.65				
20	1.44	1.44	1.44	1.45	1.50	1.59				
30	1.45	1.45	1.45	1.46	1.51	1.59				
50	1.57	1.57	1.58	1.59	1.64	1.75				
150	6.93	6.93	6.94	6.95	7.01	7.11	7.24	7.43	7.66	7.96
250	13.15	13.15	13.15	13.16	13.19	13.25	13.33	13.43	13.57	13.74
350	19.36	19.36	19.37	19.37	19.40	19.44	19.50	19.59	19.69	19.82

2. v_w = 20 mi/hr

X (km)	0	5	10	20	40	60	80	100	120	140
10	-	-	-							
20	1.64	1.65	1.69							
30	1.48	1.48	1.49	1.54						
50	1.44	1.44	1.45	1.48	1.65					
150	3.50	3.50	3.51	3.55	3.70	3.97				
250	6.61	6.61	6.61	6.63	6.71	6.84	7.04	7.39		
350	9.72	9.72	9.72	9.73	9.78	9.87	10.00	10.20	10.54	
450	12.82	12.82	12.83	12.84	12.88	12.94	13.05	13.20	13.42	
550	15.93	15.93	15.93	15.94	15.98	16.03	16.12	16.25	16.42	16.71
650	19.04	19.04	19.04	19.05	19.08	19.13	19.21	19.32	19.48	19.71
750	22.15	22.15	22.15	22.15	22.18	22.23	22.31	22.41	22.55	22.75

3. v_w = 30 mi/hr

X (km)	0	5	10	20	40	60	80	100	120	140
10	-	-	-							
20	-	-	-							
30	-	-	-							
50	1.51	1.52	1.54							
150	2.36	2.36	2.38	2.44	2.71					
250	4.43	4.43	4.44	4.47	4.59	4.83				
350	6.50	6.50	6.51	6.52	6.60	6.74	7.00			
450	8.57	8.57	8.58	8.59	8.64	8.75	8.91			
550	10.64	10.64	10.65	10.66	10.70	10.78	10.91	11.14		
650	12.71	12.72	12.72	12.73	12.77	12.83	12.94	13.12		
750	14.79	14.79	14.79	14.80	14.83	14.89	14.99	15.14	15.43	
850	16.86	16.86	16.86	16.87	16.90	16.96	17.04	17.17	17.40	
950	18.93	18.93	18.93	18.94	18.97	19.02	19.10	19.22	19.42	
1050	21.00	21.00	21.00	21.01	21.04	21.09	21.17	21.28	21.46	
1150	23.07	23.07	23.08	23.08	23.11	23.16	23.23	23.34	23.51	

Table 4A

SUMMARY OF TIME OF CESSATION OF FALLOUT FROM CLOUD HEIGHTS
AT SELECTED X,Y LOCATIONS FOR W = 1,000 KT

Y (km)

1. v_w = 10 mi/hr

X (km)	0	5	10	20	40	60	80	100	120	140
10	1.62	1.61	1.60	1.56	1.28					
20	2.24	2.24	2.23	2.20	2.05					
30	2.86	2.86	2.85	2.83	2.72					
50	4.10	4.10	4.10	4.98	4.01	3.87				
150	10.32	10.32	10.32	10.31	10.27	10.21	10.12	9.98	9.71	
250	16.53	16.53	16.53	16.52	16.50	16.44	16.37	16.25	16.08	
350	22.75	22.75	22.75	22.74	22.71	22.66	22.59	22.48	22.32	21.97

2. v_w = 20 mi/hr

X (km)	0	5	10	20	40	60	80	100	120	140
10	0.85	0.84	0.80							
20	1.16	1.15	1.13							
30	1.47	1.47	1.45	1.37						
50	2.09	2.09	2.08	2.03						
150	5.20	5.20	5.20	5.18	5.11	4.93				
250	8.31	8.31	8.31	8.29	8.25	8.15				
350	11.42	11.42	11.41	11.40	11.36	11.29	11.12			
450	14.52	14.52	14.52	14.51	14.48	14.40	14.26			
550	17.63	17.63	17.63	17.62	17.58	17.51	17.38			
650	20.74	20.74	20.74	20.73	20.69	20.62	20.49			
750	23.85	23.85	23.84	23.84	23.80	23.73	23.60			

3. v_w = 30 mi/hr

X (km)	0	5	10	20	40	60	80	100	120	140
10	-	-	-							
20	0.80	0.79	0.74							
30	1.01	1.00	0.97							
50	1.42	1.42	1.40							
150	3.50	3.49	3.49	3.47	3.32					
250	5.57	5.57	5.56	5.55	5.48					
350	7.64	7.64	7.64	7.62	7.57	7.44				
450	9.71	9.71	9.71	9.70	9.65	9.56				
550	11.78	11.78	11.78	11.77	11.73	11.64				
650	13.85	13.85	13.85	13.84	13.80	13.72				
750	15.93	15.93	15.92	15.92	15.88	15.80				
850	18.00	18.00	18.00	17.99	17.95	17.87				
950	20.07	20.07	20.07	20.06	20.02	19.95				
1050	22.14	22.14	22.14	22.13	22.09	22.02				
1150	24.21	24.21	24.21	24.20	24.17	24.09				

Table 5A

SUMMARY OF TIME OF CESSATION OF FALLOUT FROM CLOUD HEIGHTS
AT SELECTED X,Y LOCATIONS FOR W = 3,000 KT

Y (km)

X (km)	0	5	10	20	40	60	80	100	120	140
				1. $v_w = 10$ mi/hr						
10	2.16	2.16	2.15	2.11	1.93					
20	2.78	2.78	2.77	2.74	2.61					
30	3.40	3.40	3.40	3.37	3.27					
50	4.65	4.65	4.54	4.62	4.55	4.41				
150	10.86	10.86	10.86	10.85	10.82	10.76	10.67	10.54	10.36	10.07
250	17.08	17.08	17.07	17.07	17.04	16.99	16.93	16.83	16.71	16.54
350	23.29	23.29	23.29	23.28	23.26	23.22	23.15	23.07	22.96	22.81
				2. $v_w = 20$ mi/hr						
10	1.11	–	–							
20	1.43	1.42	–							
30	1.74	1.73	1.72	1.64						
50	2.36	2.36	2.35	2.30						
150	5.47	5.47	5.46	5.45	5.37	5.20				
250	8.58	8.58	8.57	8.56	8.51	8.42	8.25			
350	11.68	11.68	11.68	11.67	11.63	11.56	11.44	11.21		
450	14.79	14.79	14.79	14.78	14.75	14.68	14.58	14.41		
550	17.90	17.90	17.90	17.89	17.86	17.80	17.71	17.56		
650	21.01	21.01	21.00	21.00	20.97	20.91	20.82	20.68		
750	24.11	24.11	24.11	24.10	24.07	24.02	23.93	23.80	23.50	
				3. $v_w = 30$ mi/hr						
10	0.77	0.75	0.69							
20	0.98	0.97	0.92							
30	1.19	1.18	1.14							
50	1.60	1.59	1.57							
150	3.67	3.67	3.66	3.63	3.49					
250	5.74	5.74	5.74	5.72	5.65	5.46				
350	7.81	7.81	7.81	7.80	7.75	7.64				
450	9.89	9.89	9.88	9.87	9.83	9.75	9.56			
550	11.96	11.96	11.96	11.95	11.91	11.84	11.70			
650	14.03	14.03	14.03	14.02	13.98	13.92	13.80			
750	16.10	16.10	16.10	16.09	16.06	16.00	15.89			
850	18.17	18.17	18.17	18.16	18.13	18.07	17.97			
950	20.24	20.24	20.24	20.23	20.20	20.15	20.05			
1050	22.32	22.32	22.31	22.31	22.28	22.22	22.12	21.87		
1150	24.39	24.39	24.39	24.38	24.35	24.29	24.20	23.97		

A.7

Table 6A

SUMMARY OF TIME OF CESSATION OF FALLOUT FROM CLOUD HEIGHTS
AT SELECTED X,Y LOCATIONS FOR W = 10,000 KT

Y (km)

X (km)	0	5	10	20	40	60	80	100	120	140
				1. v_w = 10 mi/hr						
10	3.15	3.14	3.14	3.11	2.98	2.71				
20	3.77	3.77	3.76	3.73	3.63	3.42				
30	4.39	4.39	4.38	4.36	4.27	4.10				
50	5.63	5.63	5.63	5.61	5.54	5.41				
150	11.85	11.85	11.84	11.84	11.80	11.74	11.65	11.52	11.36	11.13
250	18.06	18.06	18.06	18.05	18.03	17.98	17.92	17.83	17.71	17.57
350	24.28	24.28	24.28	24.27	24.25	24.21	24.15	24.08	23.98	23.86
				2. v_w = 20 mi/hr						
10	-	-	-							
20	1.92	1.91	1.89							
30	2.23	2.22	2.21	2.14						
50	2.85	2.85	2.83	2.79	2.52					
150	5.96	5.96	5.95	5.93	5.84	5.67				
250	9.07	9.06	9.06	9.05	8.99	8.89	8.73	8.44		
350	12.17	12.17	12.17	12.16	12.12	12.04	11.93	11.76	11.45	
450	15.28	15.28	15.28	15.27	15.23	15.17	15.08	14.94	14.74	
550	18.39	18.39	18.39	18.38	18.35	18.29	18.21	18.09	17.93	17.65
650	21.50	21.49	21.49	21.49	21.46	21.41	21.33	21.23	21.08	20.85
750	24.60	24.60	24.60	24.59	24.57	24.52	24.45	24.35	24.21	24.01
				3. v_w = 30 mi/hr						
10	-	-	-							
20	-	-	-							
30	-	-	-							
50	1.92	1.91	1.90							
150	3.99	3.99	3.98	3.95	3.79					
250	6.07	6.06	6.06	6.04	5.95	5.77				
350	8.14	8.14	8.13	8.12	8.06	7.94	7.71			
450	10.21	10.21	10.21	10.19	10.15	10.06	9.91			
550	12.28	12.28	12.28	12.27	12.23	12.16	12.04	11.83		
650	14.35	14.35	14.35	14.34	14.31	14.24	14.14	13.98		
750	16.42	16.42	16.42	16.41	16.38	16.32	16.23	16.09	15.81	
850	18.50	18.50	18.49	18.49	18.46	18.40	18.32	18.19	17.97	
950	20.57	20.57	20.57	20.56	20.53	20.48	20.40	20.28	20.09	
1050	22.64	22.64	22.64	22.63	22.60	22.55	22.48	22.37	22.20	
1150	24.71	24.71	24.71	24.70	24.68	24.63	24.56	24.45	24.28	

A.8

Table 7A

SUMMARY OF EXPOSURE DOSE-STANDARD INTENSITY RATIOS
UP TO H + 36 FOR SELECTED X,Y LOCATIONS
$(W = 1,000 \text{ KT}, \bar{v}_w = 20 \text{ mi/hr})$[a]

X (km)	D_1/I_s	D_2/I_s	$D(36)/I_s$	X (km)	D_1/I_s	D_2/I_s	$D(36)/I_s$
	Y = 0 km				Y = 40 km		
10	0.331	2.54	2.87	150	0.051	1.10	1.15
20	0.438	2.21	2.65	250	0.033	0.806	0.839
30	0.446	1.99	2.44	350	0.023	0.620	0.643
50	0.241	1.70	1.94	450	0.018	0.483	0.501
150	0.065	1.08	1.15	550	0.014	0.377	0.391
250	0.038	0.801	0.839	650	0.012	0.289	0.301
350	0.026	0.617	0.643	750	0.010	0.215	0.225
450	0.020	0.482	0.502				
550	0.016	0.375	0.391		Y = 60 km		
650	0.013	0.288	0.301				
750	0.011	0.214	0.225	150	0.024	1.12	1.14
				250	0.024	0.813	0.837
	Y = 10 km			350	0.019	0.623	0.642
				450	0.015	0.486	0.501
10	0.279	2.61	2.89	550	0.012	0.379	0.391
20	0.410	2.24	2.65	650	0.010	0.291	0.301
30	0.364	2.01	2.37	750	0.009	0.216	0.225
50	0.230	1.70	1.93				
150	0.064	1.09	1.15		Y = 80 km		
250	0.038	0.803	0.841				
350	0.026	0.618	0.644	350	0.009	0.632	0.641
450	0.020	0.482	0.502	450	0.008	0.492	0.500
550	0.016	0.376	0.392	550	0.007	0.383	0.390
650	0.013	0.288	0.301	650	0.006	0.294	0.300
750	0.011	0.214	0.225	750	0.005	0.219	0.224
	Y = 20 km						
30	0.262	2.06	2.32				
50	0.192	1.72	1.91				
150	0.062	1.09	1.15				
250	0.036	0.803	0.839				
350	0.025	0.618	0.643				
450	0.019	0.482	0.501				
550	0.016	0.376	0.392				
650	0.013	0.288	0.301				
750	0.011	0.214	0.225				

a D_1 is the exposure dose to fallout cessation; Y

A.9

Fig. A1. Variation of $I(t)/I_s$ with Time After Detonation

A.10

Fig. A2.   Variation of $I(t)/I_s$ with Time After Detonation

A.11

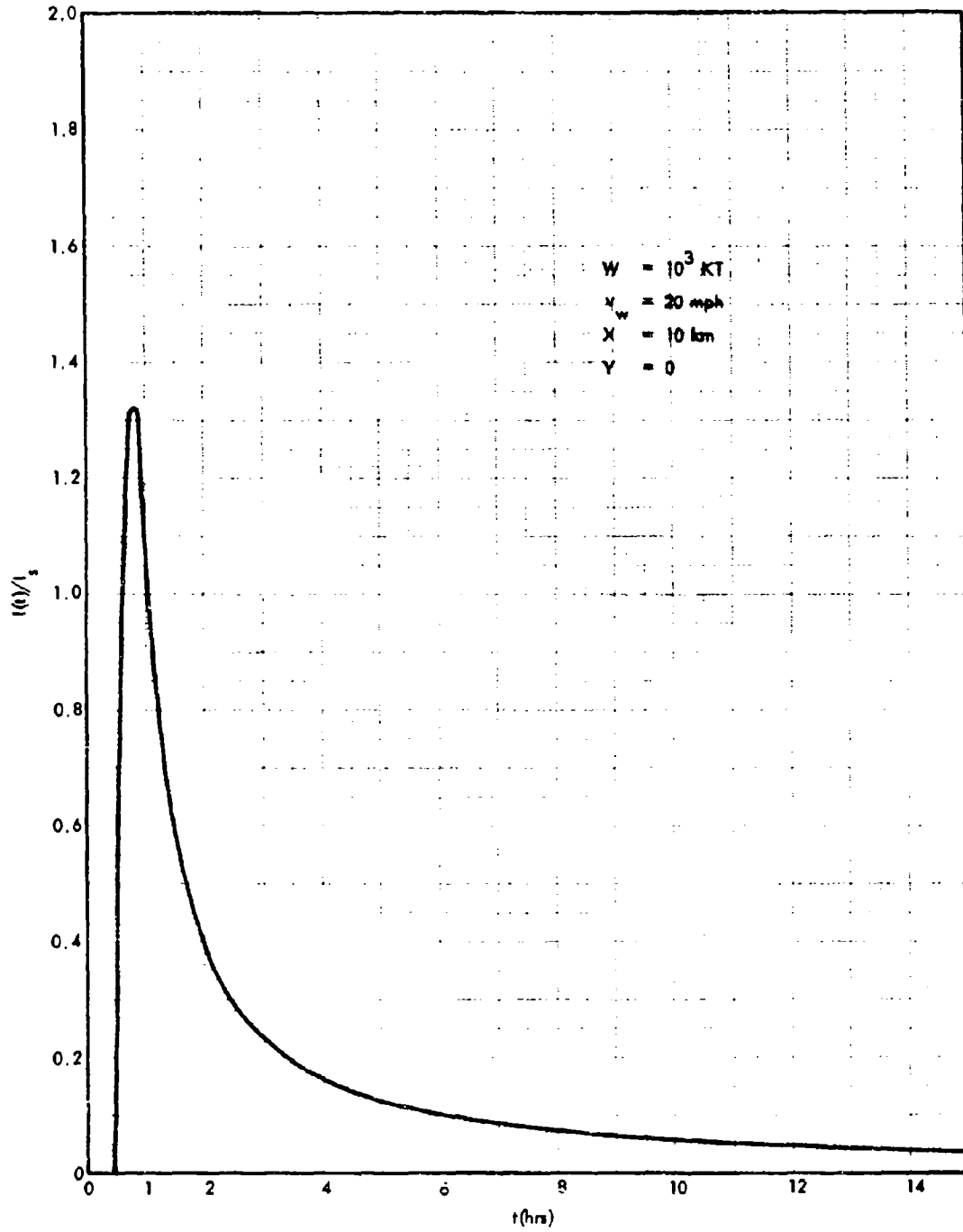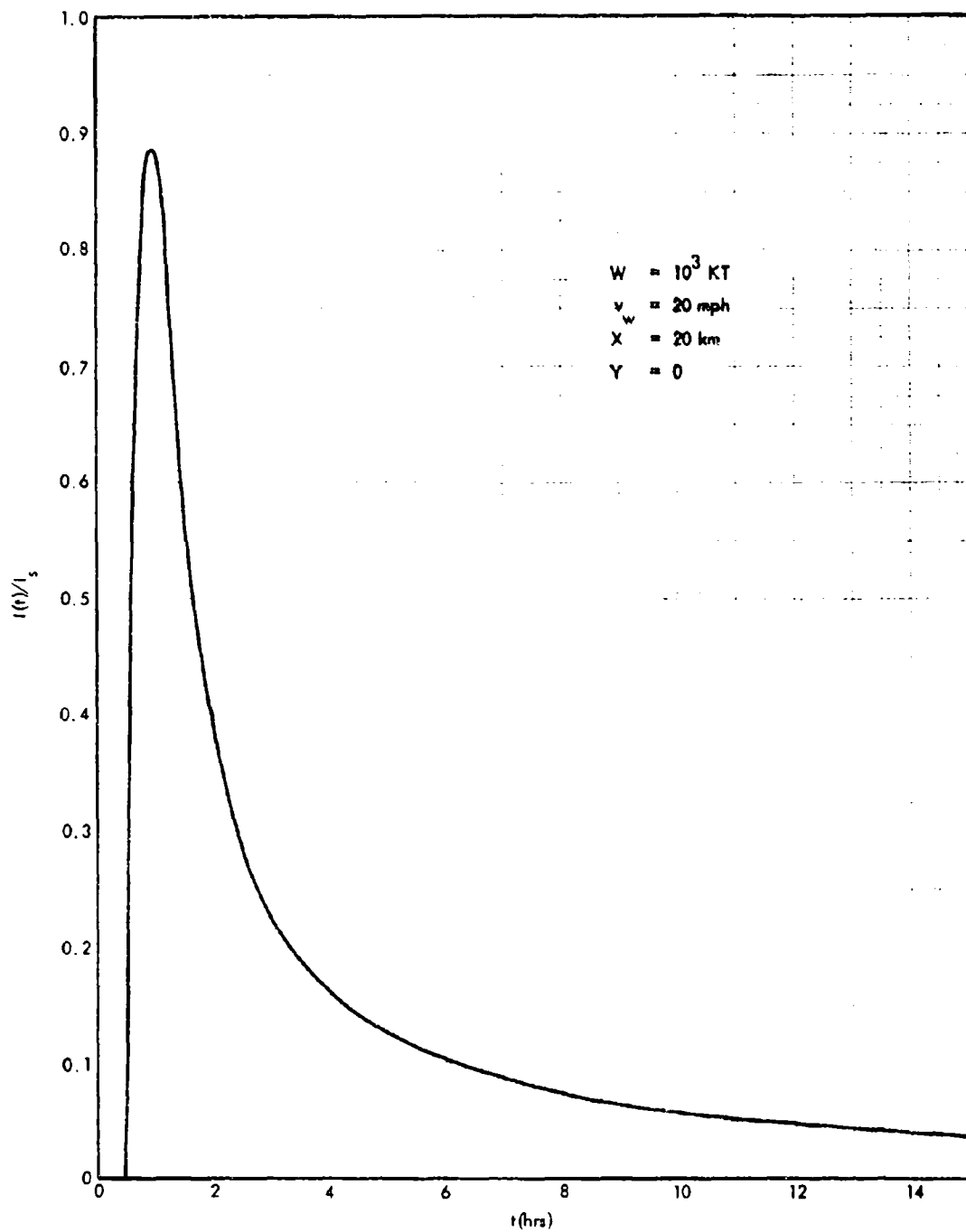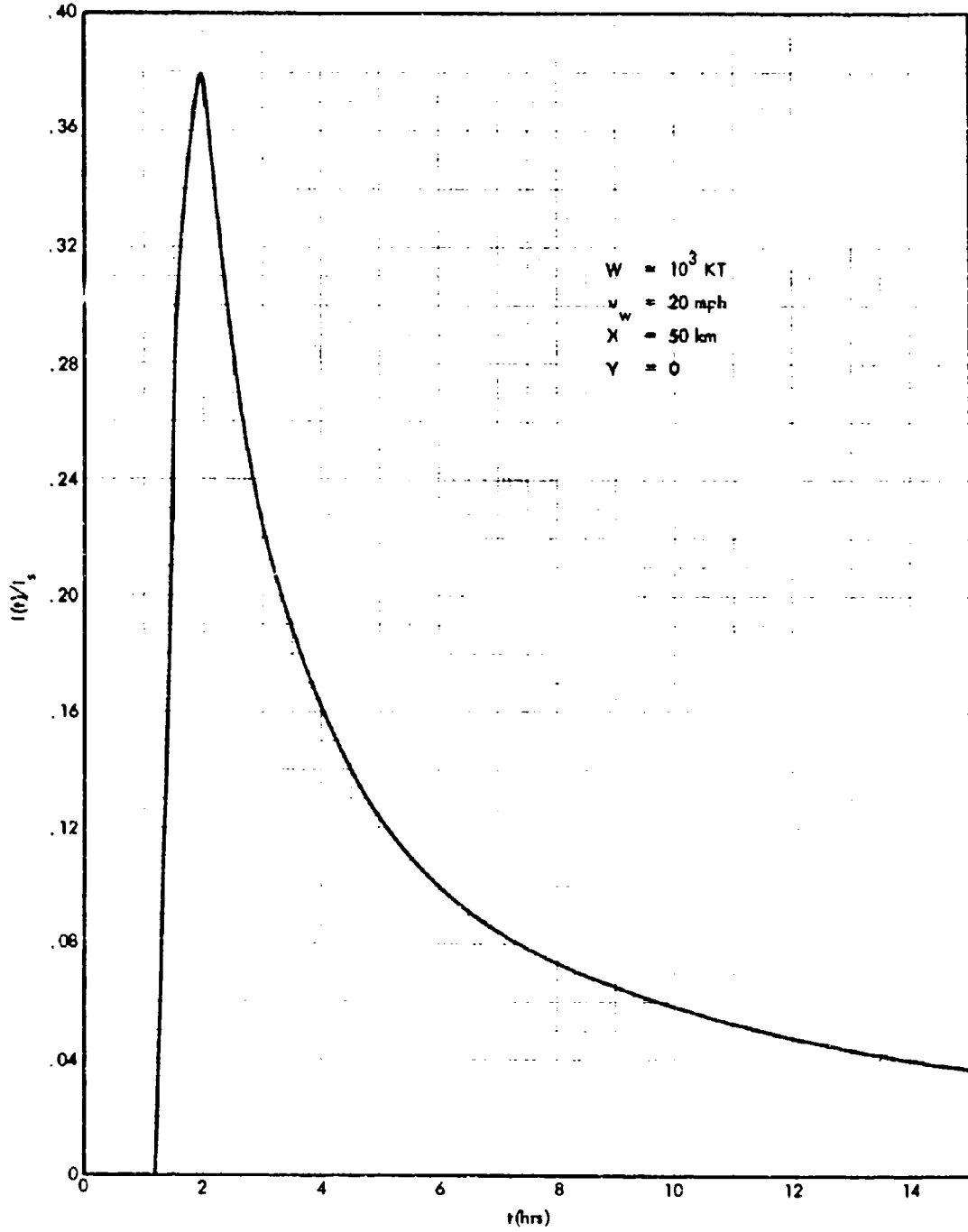Fig. A3. Variation of $I(t)/I_s$ with Time After Detonation
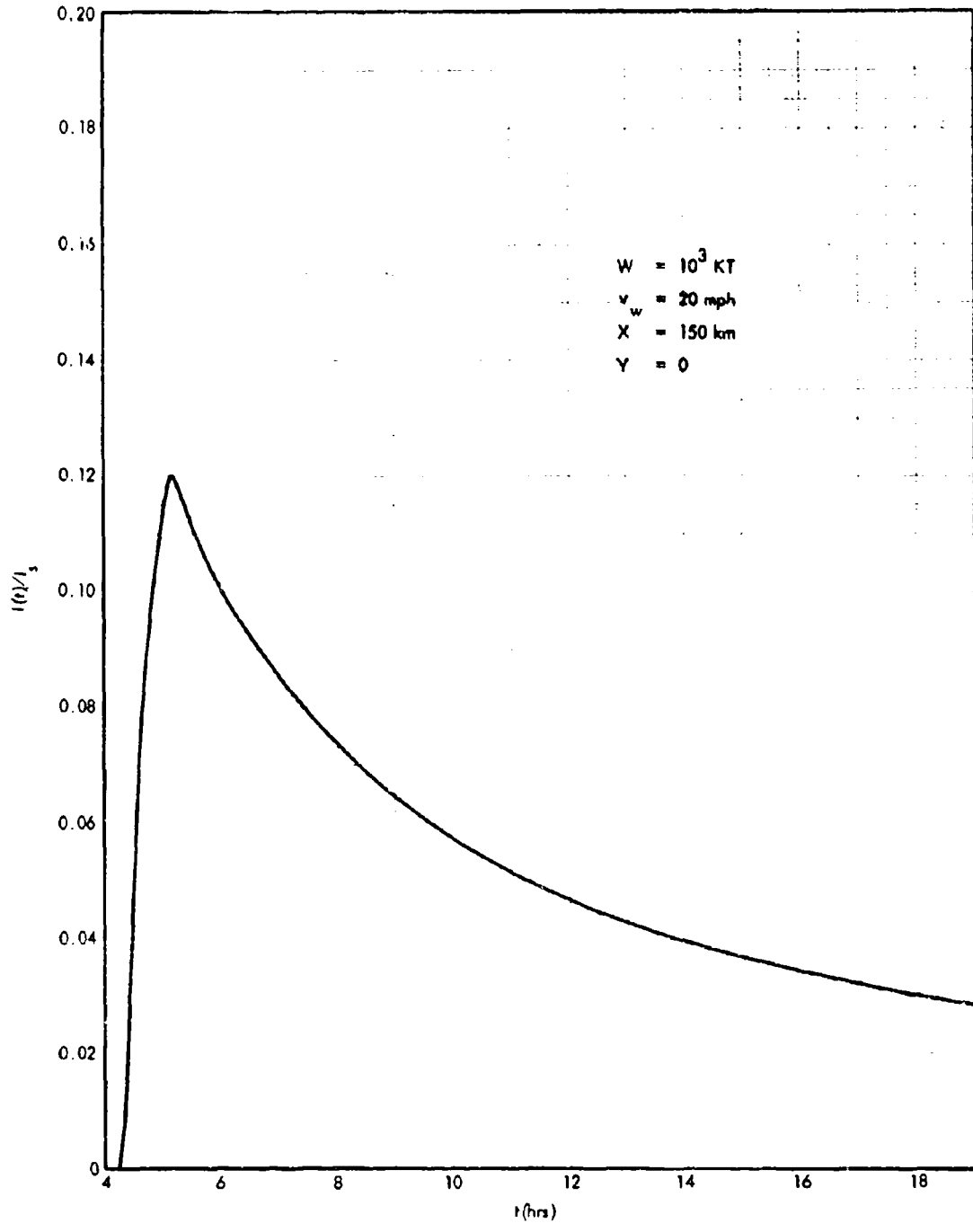
A.12

Fig. A4. Variation of $I(t)/I_s$ with Time After Detonation

A.13

Fig. A5. Variation of $I(t)/I_s$ with Time After Detonation

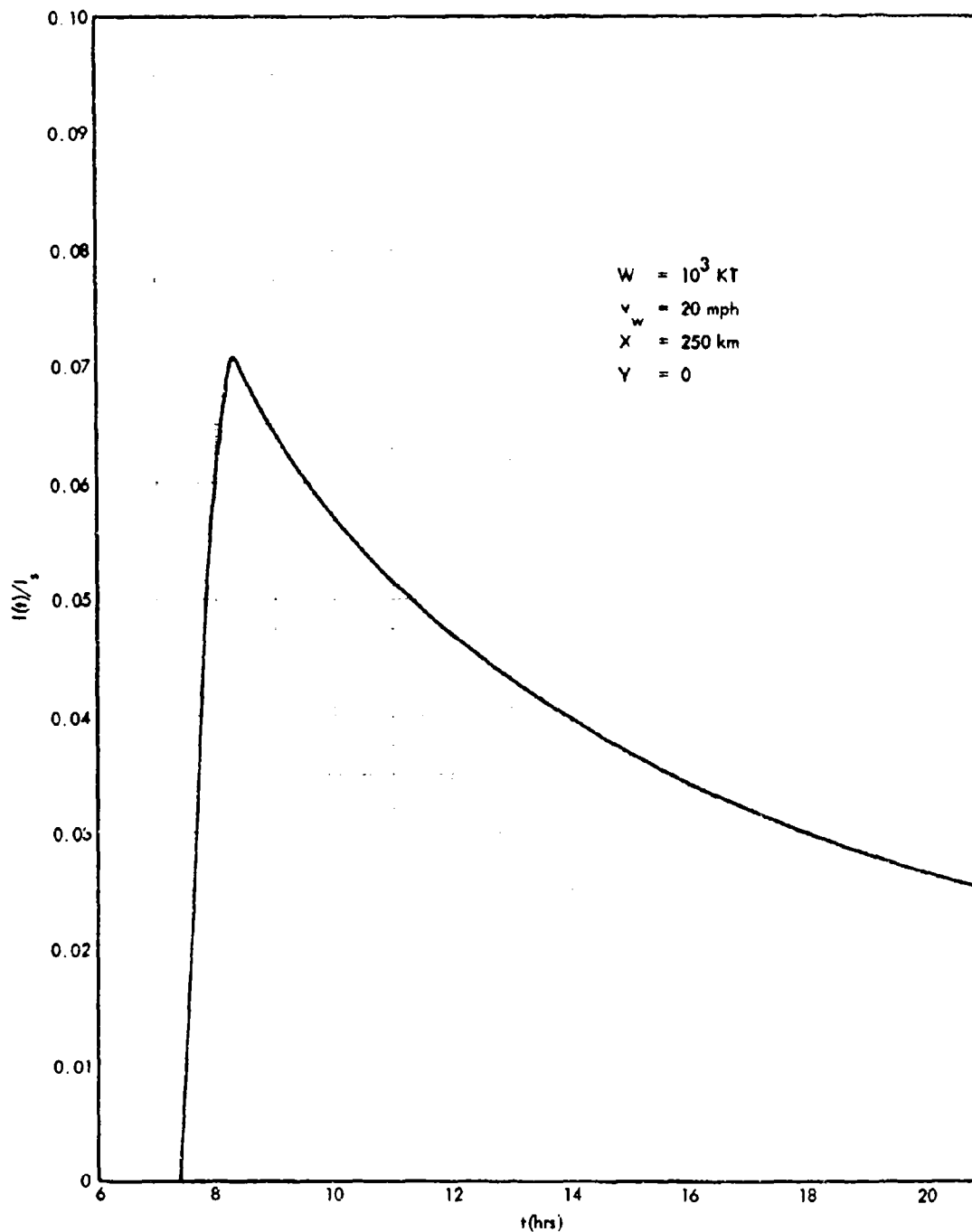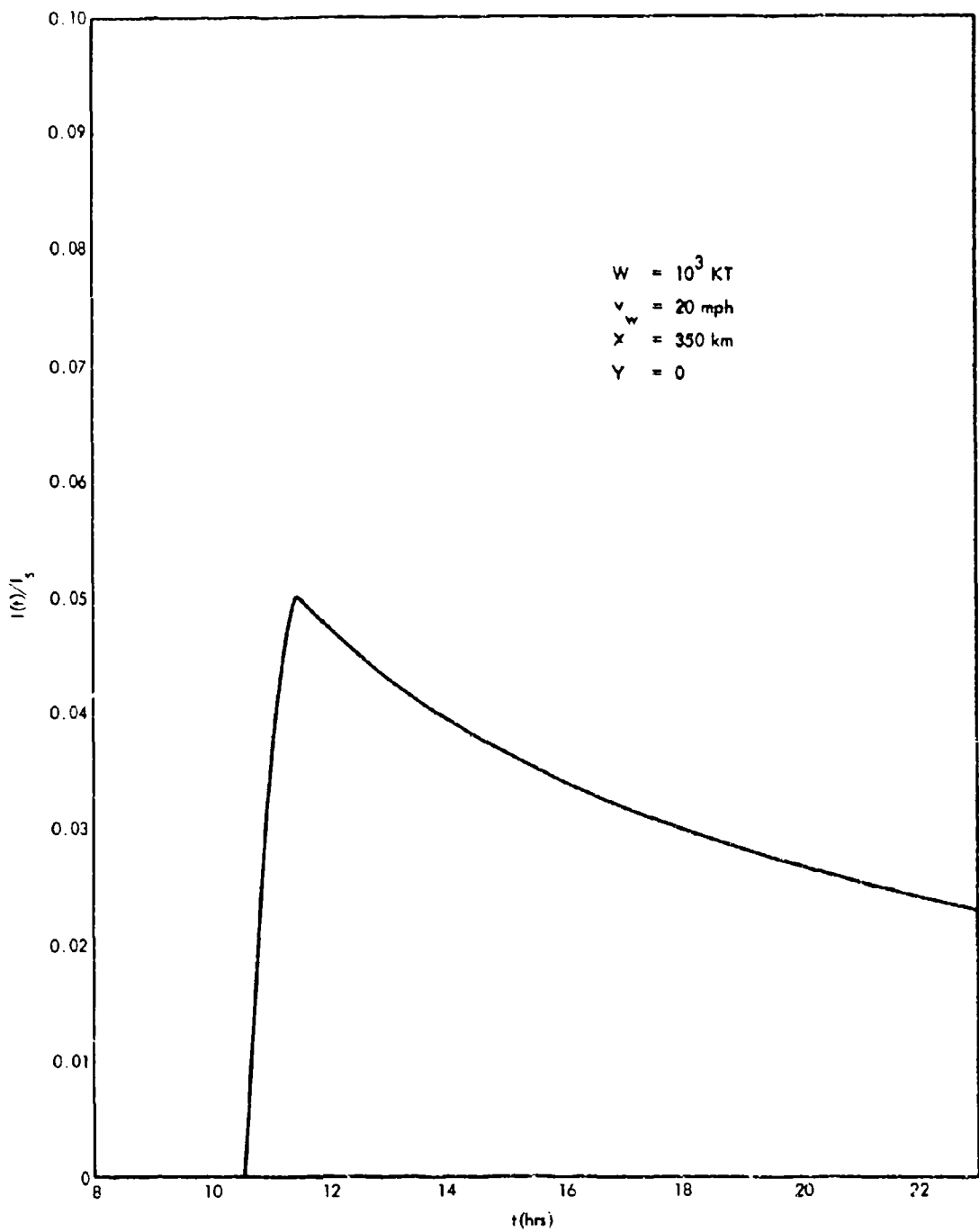Fig. A6. Variation of $I(t)/I_s$ with Time After Detonation

A.15

DOCUMENT CONTROL DATA - R & D

(Security classification of title, body of abstract and indexing annotation must be entered when the overall report is classified)

1. ORIGINATING ACTIVITY (Corporate author)	2a. REPORT SECURITY CLASSIFICATION
URS Research Company 1811 Trousdale Drive Burlingame, California 94010	Unclassified
	2b. GROUP

3. REPORT TITLE

Distribution of Local Fallout, Chapter 3, Biological and Radiological Effects of Fallout from Nuclear Explosions

4. DESCRIPTIVE NOTES (Type of report and inclusive dates)

Final Report

5. AUTHOR(S) (First name, middle initial, last name)

Carl F. Miller

6. REPORT DATE	7a. TOTAL NO. OF PAGES	7b. NO. OF REFS
May 1969	117	16

8a. CONTRACT OR GRANT NO.	9a. ORIGINATOR'S REPORT NUMBER(S)
N00228-68-C-2390	URS 702-1
b. PROJECT NO.	
c.	9b. OTHER REPORT NO(S) (Any other numbers that may be assigned this report)
d.	TRC-68-61

10. DISTRIBUTION STATEMENT

This document is approved for public release and sale; its distribution is unlimited.

11. SUPPLEMENTARY NOTES	12. SPONSORING MILITARY ACTIVITY
	Office of Civil Defense Office of the Secretary of the Army Washington, D.C. 20310

13. ABSTRACT

This report summarizes the fallout pattern scaling relationships that were developed in the period 1962 to 1964; the report includes the values of the scaling equation coefficients that were derived from selected fallout pattern data. The meaning of the scalar wind speed multiplier that is used in the scaling equations is discussed relative to computer applications of the scaling system and approximate wind speed adjustment factors for use with wind speed averages that may be assumed in such applications are provided. The relative degree of wind shear inherent in the scaling system parameters is also discussed in some detail. Basic equations for relating surface density of radionuclides and air ionization rate, including consideration of fractionation, surface roughness, and instrument response are given and discussed together with the influence of these factors and others on the limiting values of K factors that represent the relative amount of the radioactive sources contained within the deduced area covered by the fallout patterns. Scaling equations and data are also presented for use in estimating, for any location in the fallout region, the time of fallout arrival, the time of fallout cessation, the variation of the exposure rate (i.e., air ionization rate in roentgens per hour) with time during fallout arrival, and the total potential exposure from the time of fallout arrival to selected later times.

DD FORM 1473 REPLACES DD FORM 1473, 1 JAN 64, WHICH IS OBSOLETE FOR ARMY USE.

14. KEY WORDS	LINK A		LINK B		LINK C	
	ROLE	WT	ROLE	WT	ROLE	WT
Fallout						
Exposure Dose						
Exposure Rate						
Air Ionization Rate						
Radionuclides						
Radioactivity						
Fallout Scaling System						
Fallout Models						
Wind Shear						
Wind Speed						
Radiological Effects						
Residual Radiation						
Roentgens						
Fractionation						
Fallout Particles						
Particle Fall Rate						
Nuclear Detonations						
Fallout Pattern						
Fallout Arrival Time						
Fallout Cessation Time						
Isodose Rate Contours						
Civil Defense						
Ground Zero						
Standard Intensity						
Fission Products						
Induced Activity						